NUMERICAL ANALYSIS OF BERDUT LINEAR ELECTRIC MOTOR FOR TRAIN PROPULSION

by

Héctor J. Ruiz-Valle

A thesis submitted in partial fulfillment of the requirements for the degree of

MASTER OF SCIENCES
in
MECHANICAL ENGINEERING

UNIVERSITY OF PUERTO RICO
MAYAGÜEZ CAMPUS
2009

Approved by:

_____	_____
Frederick Just, PhD Member, Graduate Committee	Date
_____	_____
Gustavo Gutiérrez, PhD Member, Graduate Committee	Date
_____	_____
David Serrano, ScD President, Graduate Committee	Date
_____	_____
Hector Salas, PhD Representative of Graduate Studies	Date
_____	_____
Pablo Cáceres , PhD Chairperson of the Department	Date

ABSTRACT

This thesis investigates the performance of the Berdut linear motor for use in the propulsion of trains. This motor is part of a novel technology that uses an array of permanent magnets and iron-based materials in the stator combined with coils in the moving part that offer a simple and low-cost solution for transportation systems. Several topologies were considered, in order to gain a better understanding of the potential use of the technology for the propulsion of trains. The direction of permanent magnets and number of rails were modified from existing Berdut motors. The coils polarity switching was varied in an innovative effort to decrease power consumption and therefore increase efficiency. In order to model and analyze the motor, finite element simulations were run. A total of seven different topologies were assessed. Results from model options explored indicate that the topology titled: One single rail with a common nucleus was the best in terms of thrust force and the topologies titled: Out-of-phase and In-phase switching without irons offered superior performance in terms of efficiency when compared with the Berdut classic pole. In addition, the motors are more efficient with less coil turns in the moving part. Others studies were the effect of time step, mesh size and ripple.

RESUMEN

Esta tesis investiga el desempeño del motor lineal de Berdut, usando el mismo para propulsión en trenes. Este motor es parte de una tecnología novedosa que utiliza un arreglo de imanes permanentes y materiales ferrosos en el estator combinado con bobinas en la parte móvil, el cual ofrece una solución simple y de bajo costo para sistemas de transportación. Para obtener un mejor entendimiento de la tecnología de motores lineales Berdut y su aplicación a la propulsión de trenes varias topologías fueron consideradas, en las cuales la dirección de los imanes permanentes y el número de vías fueron modificadas en comparación con los motores de Berdut existentes. El cambio en la señal impartida a las bobinas siguió un esfuerzo innovador para disminuir el consumo y por lo tanto aumentar la eficiencia. Para analizar el motor, se usaron simulaciones en elemento finito. Un total de siete configuraciones fueron evaluadas. Los resultados mostraron que la topología con el núcleo en común producía la mayor fuerza de empuje. Además, las dos configuraciones sin material ferroso entre los imanes en el estator obtuvo la más alta eficiencia. Al compararlos entonces con el motor que utiliza el polo clásico de Berdut se puede apreciar que estas configuraciones tienen mejor desempeño. En adición, se descubrió que los motores son más eficientes cuando sus bobinas tienen el menor número de vueltas.

DEDICATION

This work is dedicated to my wife Yolanda for all her support, comprehension and love that gives me the day-to-day motivation.

ACKNOWLEDGEMENTS

During the development of my graduate studies at the University of Puerto Rico several persons collaborated in different manners with my investigation. Without their support it would be impossible for me to finish my work. That is why I wish to dedicate this section to recognize their support.

First of all, I want to truly acknowledge my thesis advisor, Dr. David Serrano for explaining and guiding me during all the steps to complete my degree. Those steps included the technical and administrative issues and also the opportunity to assist to conferences and be exposed to the professional world of research. I also want to extend these acknowledgements to my graduate committee members: Dr. Frederick Just and Dr. Gustavo Gutierrez. They also contributed in helping me in my development by their disposition and critical advice. In addition, I want to give thanks to Mr. Ezequiel Medici for his help and advice in the finite element modeling and analysis. Finally, it is of special relevance to acknowledge Mr. E. Berdut, patent inventor of the object of study of this and many other works. His accessibility, motivation, advice and patience were very significant to me.

Table of Contents

Figure List

Figures **Page**

1 INTRODUCTION

1.1 Motivation

Electric motors have been of great impact in the industry and the home due to their practical applications. From appliances to power tools, from spacecrafts to automotive, electric motors are very common machines. In addition to their different functionality, their power-to-density ratio and their high efficiencies are key issues.

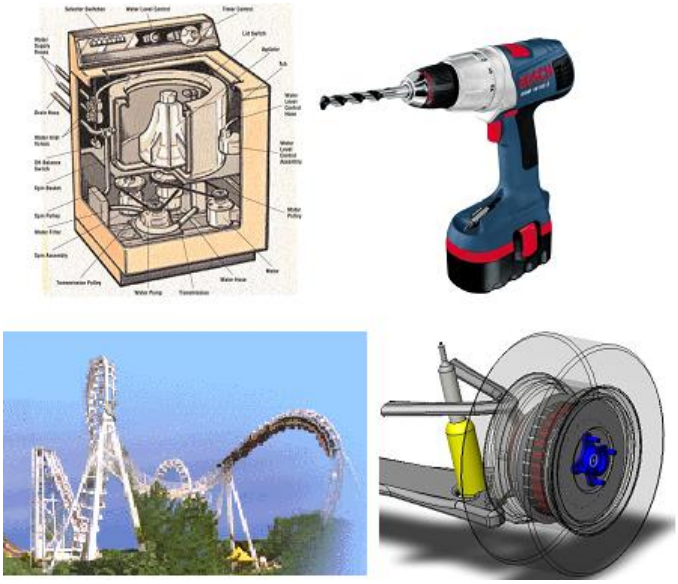

Figure 1.1: Typical applications in which motors are found: top left - home appliances; top right - tools; bottom left - entertainment; bottom right - transportation

Magnetic Levitation, or MAGLEV – Figure 1-2, are trains that use sets of coils and magnets to setup a magnetic field that suspend, guide and propels them. There are different types and their differences are based on the arrays used for these functions.

Figure 1.2: Example of a MAGLEV train

Among the different MAGLEV technologies, there are: Electromagnetic, Electrodynamic, Indutrack and Berdut. A brief explanation of each one follows:

1. Electromagnetic suspension (EMS) – This system, shown in figure 1-3, contains electromagnets on both the train and the rail. The ones on the train are continuously energized, while the rail coils turn on when the moving electromagnets are passing by. The same array of electromagnets provides the levitation, guidance and propulsion by attraction of the magnetic fields [8, 14].

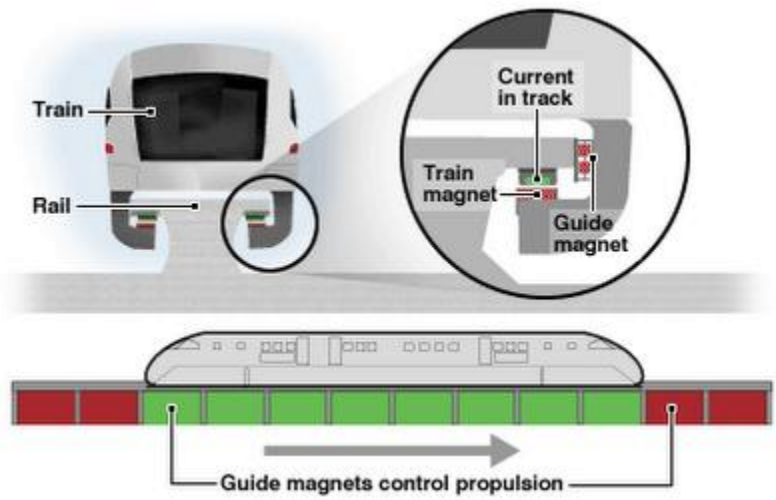

Figure 1.3: Electromagnetic levitation and guidance schematic

2. Electrodynamic suspension (EDS) – The second type of MAGLEV is known electrodynamic suspension. Levitation is due to repulsive forces between the static and moving objects. A separate system is used for propulsion, which is a linear motor that has its current synchronized with the train speed. The rails contain the levitation and propulsion systems with two different sets of coils, as shown in Figure 1-4(a). These coils induce magnetic fields opposite to the moving member, as shown in Figure 1-4(b). The result is a continuous flow of repulsive and attractive forces that keep the train moving [8, 15].

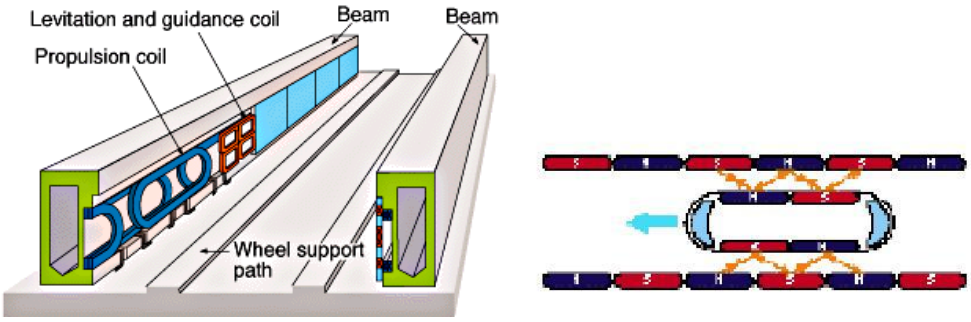

(a) **(b)**

Figure 1.4: EDS. 1-4(a): Components of the rail, showing the two different coils for levitation and propulsion, respectively. 1-4(b): Logistic in propulsion.

3. Indutrack – This system acts also by repulsion. Figure 1-5 shows a general layout of its components and principle of operation. Permanent magnets are located in the car while passive coils are in the track. One array of coils provides levitation while the other provides guidance. A third array would provide propulsion.

   A Halbach array is used to install the permanent magnets. It concentrates the magnetic field on the side facing the track coils while canceling it at the side pointing to the passengers. These coils are passive because they are not electrified. Their current is induced by the movement of the permanent magnets of the car. That's why is called Indutrack (Indu: induction). Furthermore, that induced current generates a magnetic flux in the opposite direction that in turn produces the levitation.

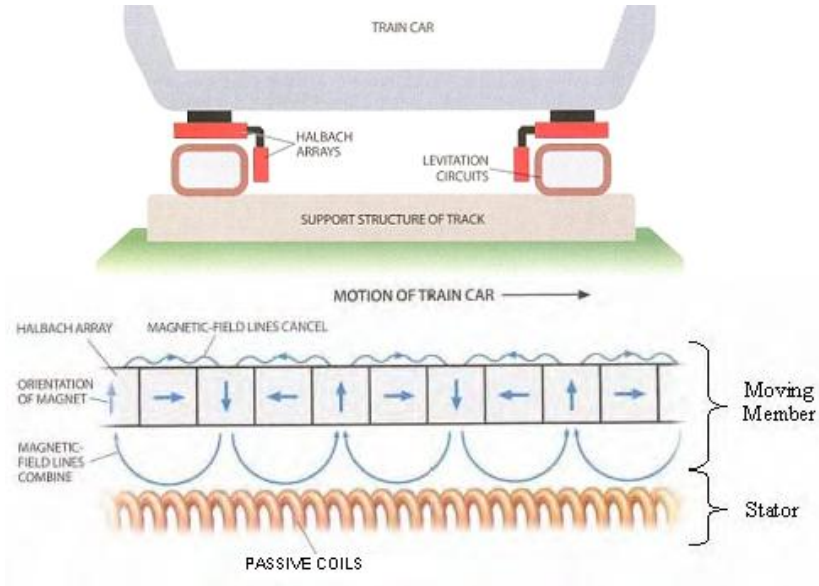

Figure 1.5: General layout of the components and principle of operation of the Indutrack MAGLEV

4. Berdut technology – Among the existing technologies for electromagnetic propulsion and levitation, the Berdut technology offers an innovative solution that does not rely in the cost and complexity of existing systems [2, 16, 17, 18, 19]. Figure 1-6 shows how it is used in a train. Levitation skates are mounted in two set of rails, one at each side. There are permanent magnets at both the rail and the car in such a way they are in attraction with the adjacent pole and in repulsion with the pole before or after it. Figure 1-7 shows graphically that attraction and repulsion interaction. Any attempt to unbalance the system will be opposed by this arrangement with an opposite force that will maintain equilibrium. The center rail contains the linear motor. This device also has permanent magnets in the stator and a set of coils in the moving part. A more detailed representation of the levitation skate and the linear force is shown in figure 1-8.

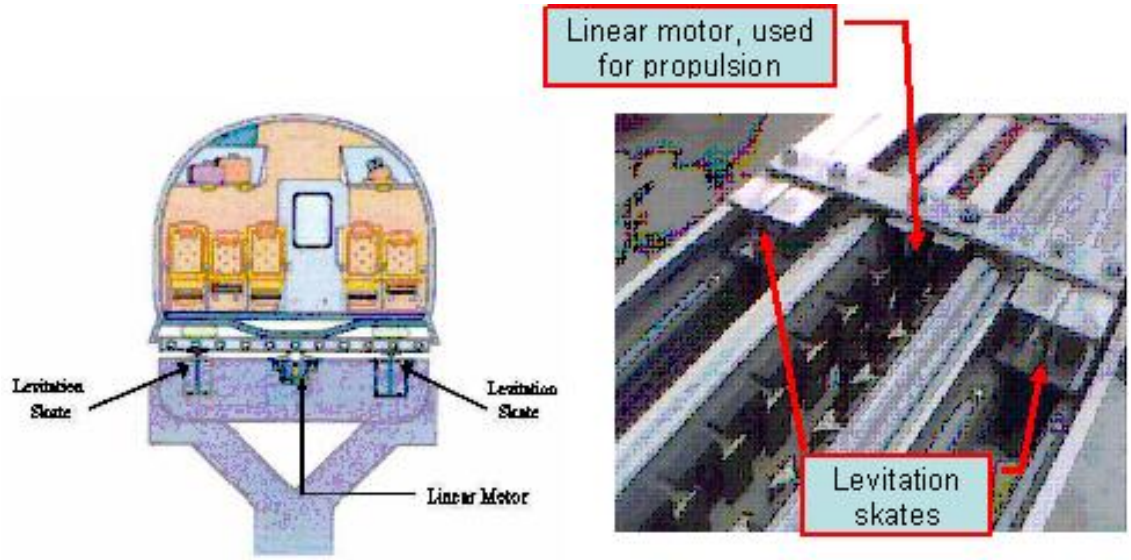

Figure 1.6: Berdut Technology used in levitation and propulsion of MAGLEV train. 1-5(a): Artistic diagram of the suspension and linear motor. 1-5(b): Picture of prototype.

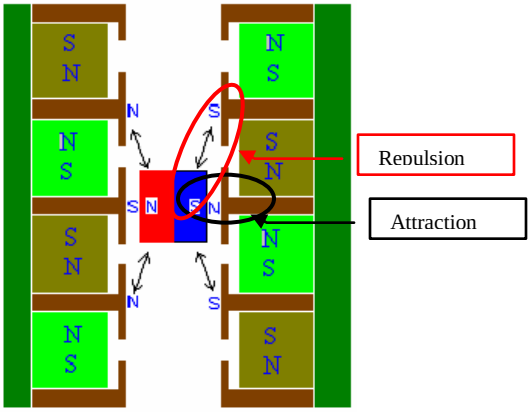

Figure 1.7: Interaction of forces in Berdut technology. There is attraction between adjacent poles at the car and rail and repulsion in poles adjacent to them

Figure 1-8 shows a 3D view of the Berdut systems described above in order to help visualize this technology. The skate and stator of 1-8a are used for levitation and

guidance and the rotor 1-8b is used for propulsion. This investigation will focus in the propulsion system.

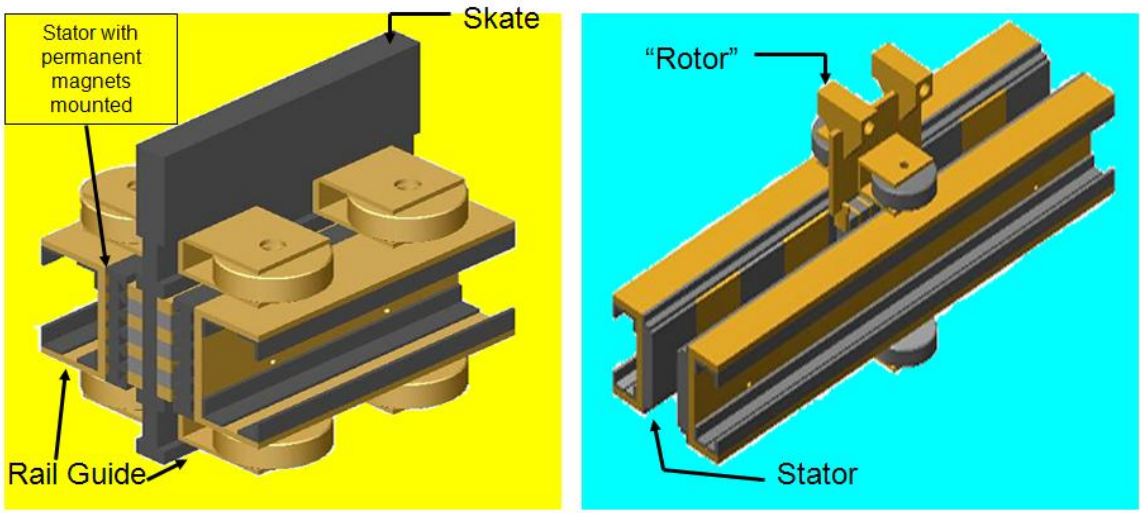

Figure 1.8: Berdut 3D models. Figure 1-8a at the left is for levitation and guidance. This version uses wheels for guidance but they can be replaced by permanent magnets. Figure 1-8b is for propulsion.

Figure 1-9 shows the taxonomy of electric motors. The two highest levels are according to the input current: alternate or direct. Then, they are subdivided according to their topologies [23]. Due to the fact the scope of this thesis is focused only on the Berdut technology, not all of the classifications will be discussed. Only the AC Induction, the DC Brushed, DC Brushless and the Linear Motors will be discussed in order to present the similarities and differences of these motors and the Berdut technology.

The main difference from the Berdut motor studied in this investigation and the existing electric motors is that Berdut is a linear DC motor and the taxonomy only has linear AC motors. Berdut's linear DC motor does not match with any of the existing classifications,

therefore it has the potential of being developed as a unique classification. Furthermore, its performance should be assessed.

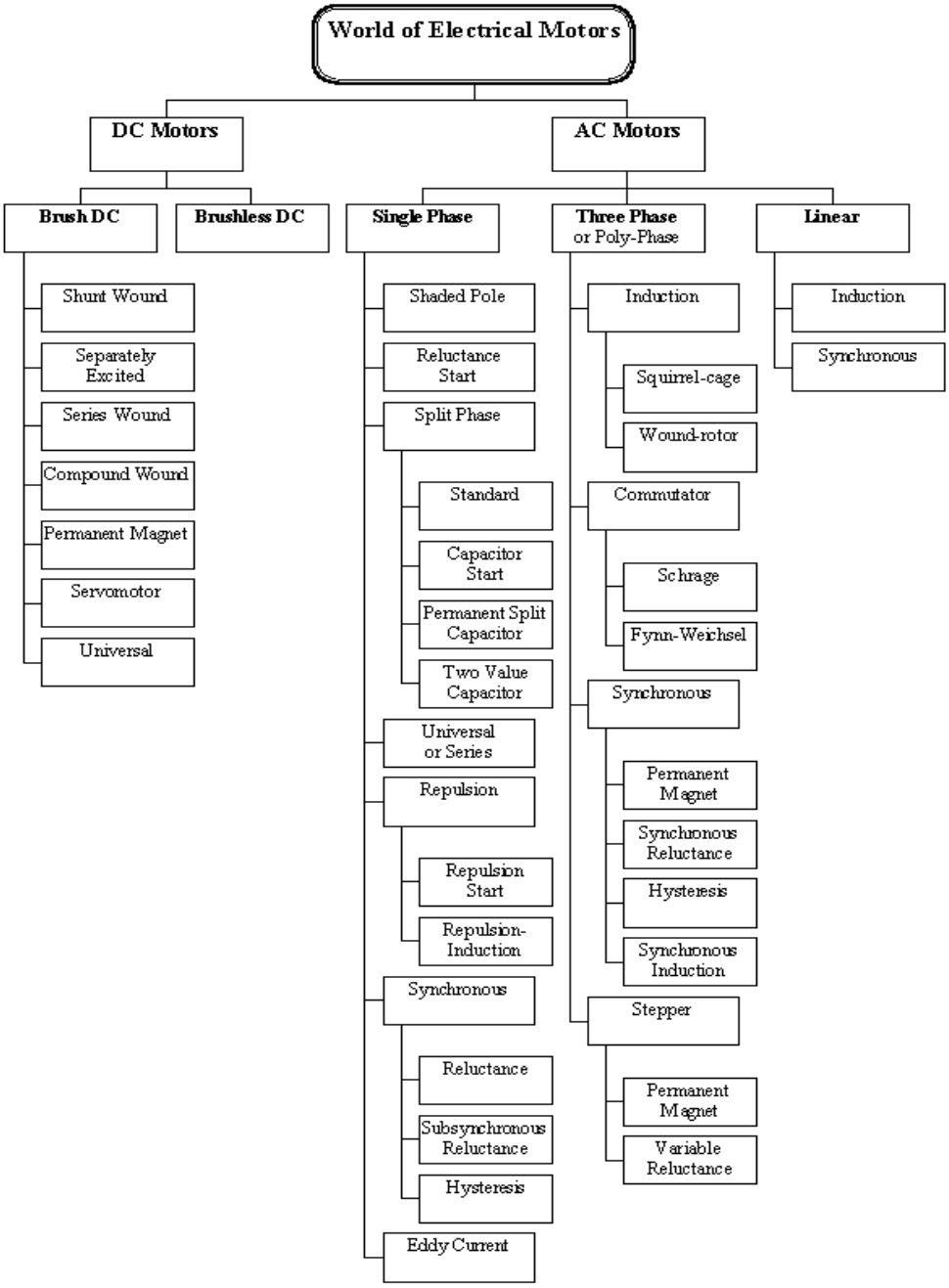

Figure 1.9: Taxonomy of Electric Motors

This thesis assesses different linear motor configurations based on Berdut Technology in order to investigate their performance and suitability for train propulsion. These will be compared against existing configurations of this and others technologies. The motor modeling will be focused on developing innovative the topology configurations and modes of operation in an attempt to obtain significant improvements to the basic Berdut linear motor. In addition, coils characteristics and permanent magnet materials that may lead the optimum efficiency, force and velocity as be applied to train propulsion will be explored.

1.2 Objectives

This work is intended to fulfill the following objectives:

1. Develop and analyze innovative topologies configurations of the Berdut Linear Motor. Those topologies differ in permanent magnet orientation, location, magnetic concentrator shapes and materials. The output variables will be the efficiency, force and velocity.
2. Analyze the effect of different switching strategies in the coils with the purpose of improving the performance of the motor with respect to the above mentioned output variables.
3. Apply the findings to a case study based on train propulsion using the combination of topology and coils characteristics that exhibit the best performance.

1.3 Methodology

In order to comply with the objectives of this investigation, the following steps will be followed:

1. Understand the theory and principle of operation related to Berdut orbital and linear motors.
2. Review literature concerning other types of linear motors under investigation and/or commercialized.
3. Investigate the theoretical background on electric motors. Study the governing equations, initial and boundary conditions and any other assumption that apply in the interaction of a moving magnetic field.
4. Develop a numerical model based on the Finite Element formulation to solve simultaneously the equations of motion and the magnetic field. First, a model with one coil will be made to setup different parameters in the analysis software such as: the current input signal, the drawing limits, initial position, solution and mechanical setup. Then, complexity will be added as more coils will be incorporated into the model.
5. Analyze results in order to identify and understand the reasons for the motor's behavior.

1.4 Literature Review

Electric motor technology dates back to 1821, when Michael Faraday demonstrated their application. He constructed the homopolar motor. Figure 1-10 shows a diagram of how it

is constructed and works. An electric current source, such as a battery, is connected to a magnet by means of a cable. There is a magnetic field ***B*** that act in the vertical direction. A current ***i*** flows through the cable. Then, by the right hand rule, a force ***F*** is generated at the cable on each side of the battery. That force is perpendicular to ***B*** and ***i*** and generates a couple that spin the cable [24].

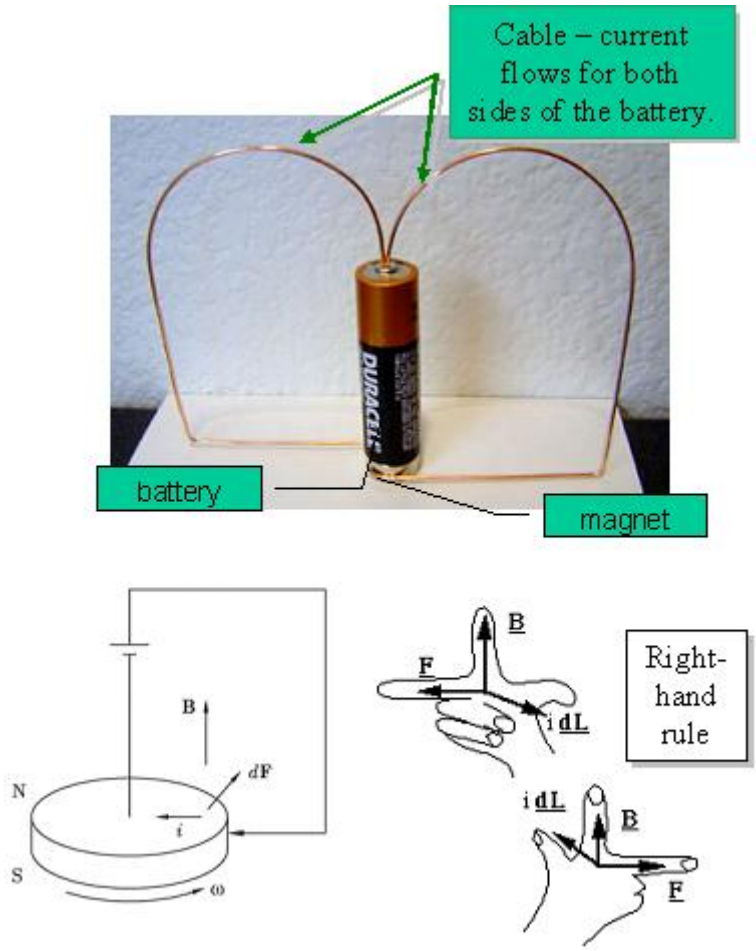

Figure 1.10: Homopolar motor form Michael Faraday

In 1831, he and Joseph Henry discovered the induction law of electromagnetism. It consists in an electric current that is generated due to a moving magnetic field that in turns generates a second magnetic field, opposite in direction. More details are given in section 2-1.

Applications of linear motors appeared in1905 with the US patent 782312 by Alfred Zehden. In 1935, Hermann Kemper built a scale working model. Then, at the end of the 1940's decade, Eric Laithwaite created the first full-size working model [8].

In general, an electric motor is a device that takes electrical power and transforms it into a mechanical movement and force by means of the interaction of magnetic fields and current-carrying conductors. That movement can be either rotational or linear. Among the different types of motors, the AC Induction, brushed DC and brushless DC, all which provide both types of motion: linear and rotational.

A brief description of each of them follows:

1. AC Induction Motor – Figure 1-11 shows the different components of this type of motor. It is made by three windings in the stator and a simple rotor. The alternate current, supplied by the stator induces a current in the rotor. Then, by Faraday's Law of induction a force is generated in a plane perpendicular to both the magnetic field and the current. That force is tangent to the rotor and therefore

makes it spin. The synchronous speed, or speed of operation, is determined by the amount of winding sets, or poles, the current frequency and the applied load. The formula that relates that speed ω_s with the number of poles n and frequency f is:

$$\omega_s = {}^{120*f}\!/_{n} \quad \textbf{(1.1)}$$

AC Induction motors advantages include: simple design, low cost, high reliability, high power, torque and efficiency. Several disadvantages include: expensive speed control and inability to run at less of 1/3rd of the synchronous speed. This motor is used when more than ½ HP is needed. Typical efficiencies exceed 90%. Figure 1-12 shows a plot of power output for different AC Induction motors configurations [8, 10, 11].

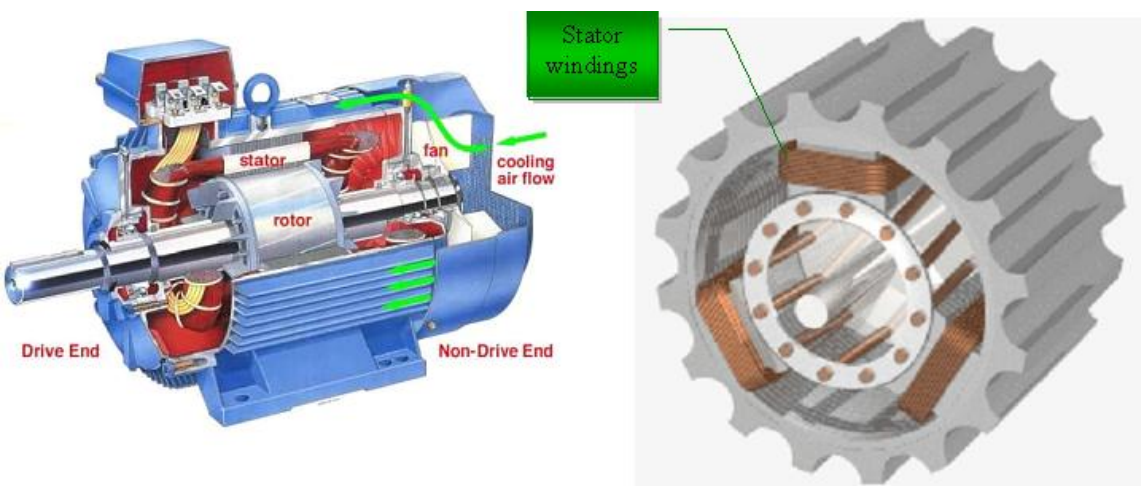

Figure 1.11: AC Induction Motor

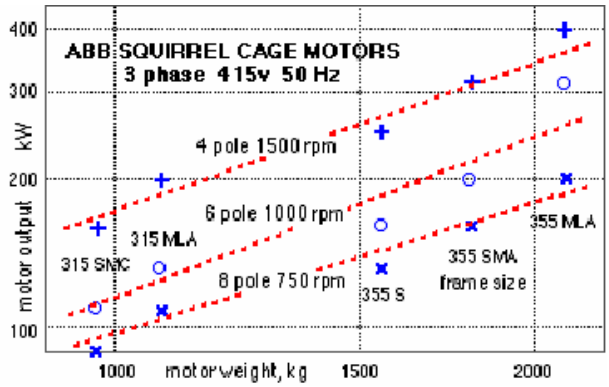

Figure 1.12: Induction Motor Performance

2. Brushed DC Motor – Please refer to Figure 1-13 for the different components of this motor and how its works. The stator is made either by permanent magnets or electromagnetic windings. The rotor poles electromagnets will try to align with the stator field. However, current changes its polarity by means of a commutator, making the motor continuously in motion. That commutator receives the energy by mechanical contacts between brushes in the rotor and rings in the stator. Its advantages are low initial cost and easy to understand control system. The main drawbacks are high maintenance and low lifespan. They are used in fractional motors, with power less than 1HP [8, 10].

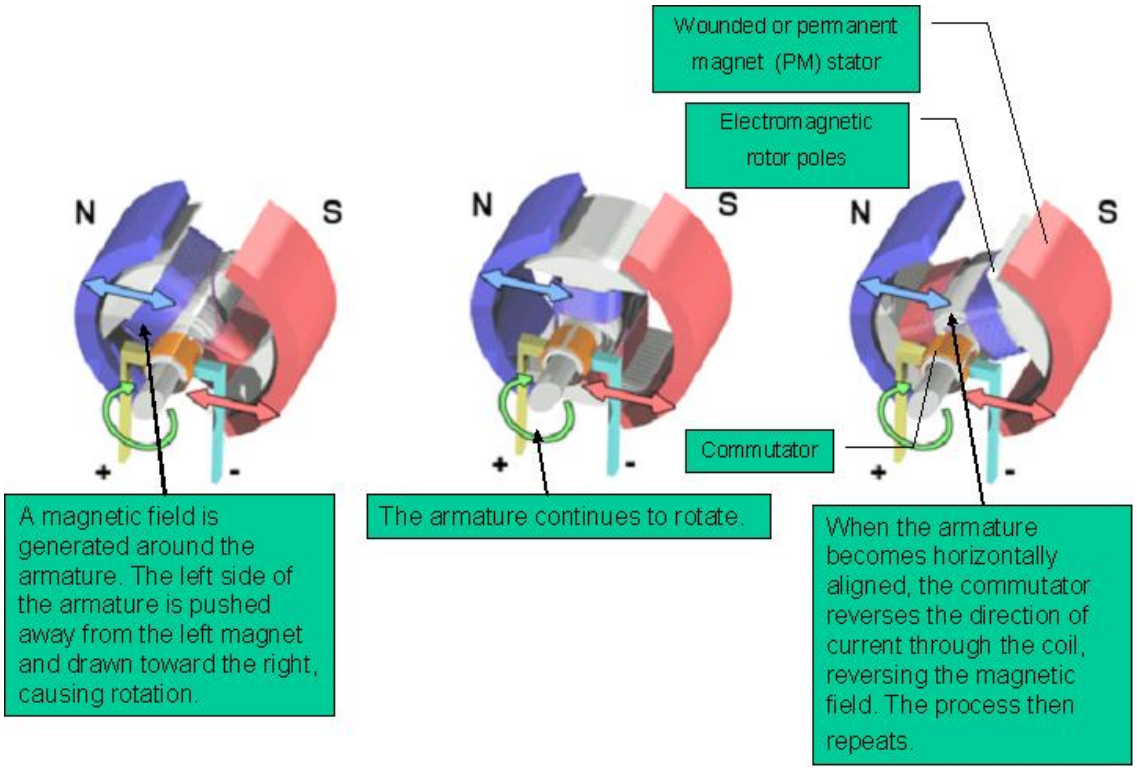

Figure 1.13: Components and principle of operation of DC Brushed Motor

3. Brushless DC Motor – The magnetic interaction is the same as the brushed motor, refer to figure 1-14. However, permanent magnets are placed in the rotor and windings in the stator. Also, the mechanical commutation is replaced by an electronic controller. The controller is composed of a sensor to measure the rotor position and an electromagnetic switch. Examples of rotor position measurements systems are the Hall-effect and the Back-EMF. The Hall-effect sensor measures the position as a function of the electric field produced when a charge is moving. The Back-EMF tells when the magnet has just passed the coil. Then, the current is switched at the exact time by means of a transistor, such as MOSFETs. They

endure more servicing time and need less maintenance than their brushed motors. However, their initial cost is higher than the brushed motors, although the advancements in electronics have decreased considerably that inconvenience. Power ranges are also less than 1HP. However, they have been considered for higher power applications, such as hub motors which deliver an average of 40HP [8, 10].

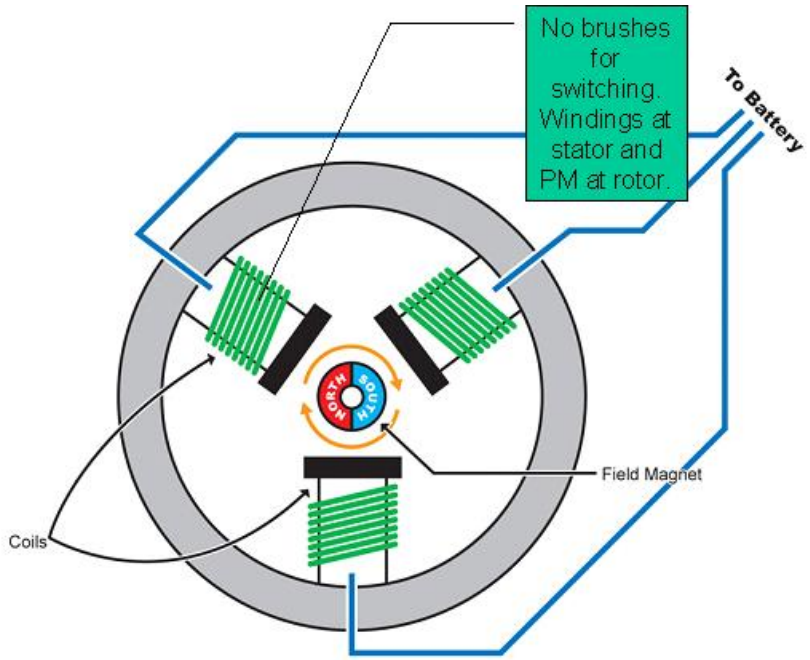

Figure 1.14: Brushless DC Motor

4. Linear motors – This type of motor operates in the same way as orbital motors do. However, the output is force instead of torque, which follows the Lorentz law of electromagnetic force [2]:

$$F_l = \rho(E + \dot{x} \times B) \quad \textbf{(1.2)}$$

In this equation, ρ is the charge density, E is the electric field, $\dot{x}$ is the velocity and B the magnetic flux density. Figure 1-15 shows how these variables relate in order to generate a force. A charge q distributed over a volume creates a charge density ρ. When it is subjected to an electric and magnetic field, a force is generated perpendicular to the velocity and each of those fields.

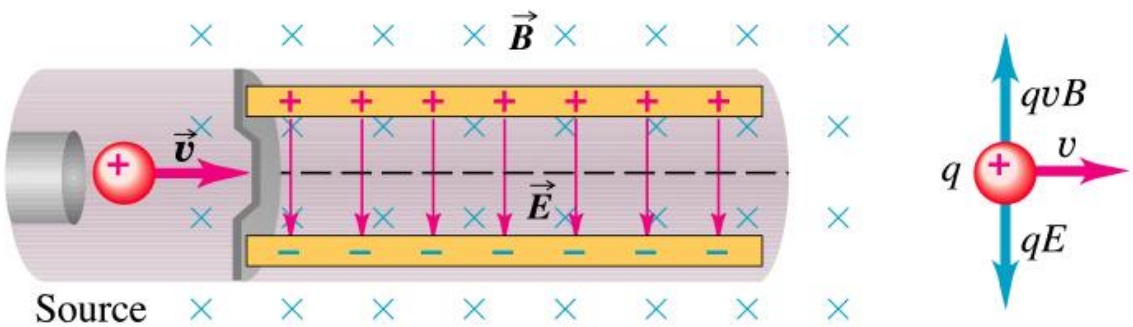

Figure 1.15: Lorentz Force over a charge

Figure 1-16 shows a general diagram of a linear motor and its relationship with the orbital motor. The movable part can be either the primary or the secondary, depending on the application.

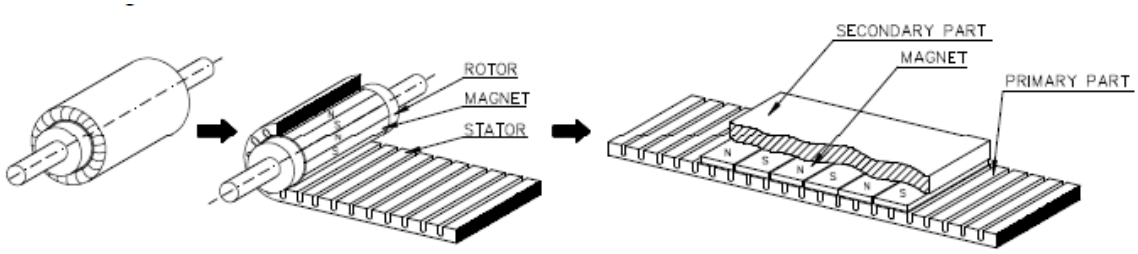

Figure 1.16: General diagram of a linear induction motor

Linear AC motors are classified as Induction or Synchronous. Each of their characteristics is explained below:

- Linear AC Induction Motor
  - Inductive motors propel a conductive reaction plate (or wound rotor coil) along a moving magnetic field by inducing a secondary magnetic field in the rotor. Magnets located at stator and coils at rotor. Figure 1-17 shows the different components.
  - The rotor is a nonmagnetic conductor such as aluminum or copper.
  - In order to get a strong enough induced magnetic field it is common to back the conductor with an iron backing plate which serves to amplify the magnetic field induced in the coil.
  - The speed of an induction motor is also determined by the line frequency, but frequency is less critical than with the synchronous motor.

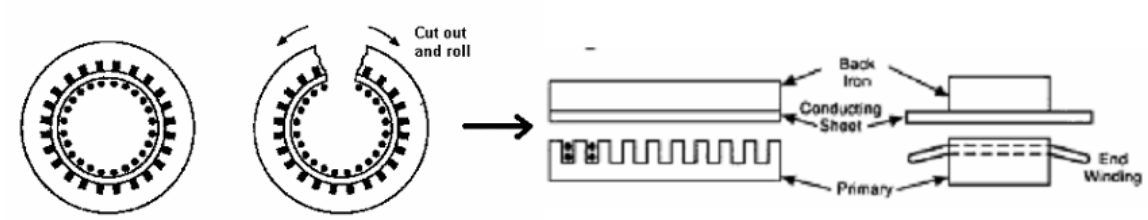

Figure 1.17: Induction Linear Motor Components

- Synchronous AC linear electric motor
  - The winding is contained in the primary part while NdFeB permanent magnets are located in the second one. Magnets at the stator and coils at the rotor.

- Can operate with a larger air gap due to the fixed magnetic field in the reaction plate.
- For efficient operation, coil timing (power line frequency) is critical to the operation of a synchronous motor.

In addition, the following notes apply for both types of motors:

- Both for efficiency and to prevent the motor coils from overheating, linear motors work best if the stator coils are switched out when the rotor is not present.
- The synchronous speed of either motor is also determined by the pole spacing in the stator units.

In addition, linear motors can be classified in two groups, according to their accelerations:

1. High-acceleration – Most of them are three-phase induction motors in which one side has the windings and the other one a passive conductor plate. They are short and their purpose is to provide the object with a high acceleration and then release it. For example the California Screamin' roller coaster goes from 0 to 55 mph in 4 sec. Others applications include weapons and plane catapults.

Figure 1.18: Examples of high acceleration linear motors

2. Low-acceleration – They are synchronous motors most commonly used in transportation, especially train propulsion. They offer the advantage of eliminating compartments for driver and large internal combustion engines. Thus, trains are smaller and lighter than conventional ones, giving the advantage of using in less space and offering more passenger capacity per train size. Examples of different configurations are:
    a. Propulsion with conventional rails – It consists of a train that contains a conductive strip between the rails that produces magnetic forces. Figure 1-19 shows Siemens Light Rail S70. It is an example of the use of linear motors with conventional rails. Top speed is 66 mph with a capacity of 220 passengers. The linear motor consists of a separate rail. The movable part is electrified.

Figure 1.19: Application of a linear motor in propulsion using conventional rails

b. Monorails – These trains have a single support and guidance structure. They can be straddle-beam o suspended monorails. They are moved by electric motors fed by dual third rails, contact wires or electrified channels attached to or enclosed in their guidance beams. The linear motor operates in EMS or EDS, as explained in section 1.1. Figure 1-20 shows a straddle-beam and a suspended monorail.

Figure 1.20: Monorails Applications

c. MAGLEV – This acronym means magnetic levitation and came from the fact that the train does not touch the rail. Instead, it uses sets of coils and magnets to setup a magnetic field that suspend and guide the train. Also, a linear electric motor propels it. The most known MAGLEV, the Transrapid in Shangai, China has a maximum speed of 269mph and seats up to 440 passengers.

Figure 1.21: Transrapid MAGLEV

d. Berdut Linear DC Motor - The ingenious arrangement of magnets and metal T's provide the magnetic lens that focuses the magnetic flux lines. A suitable rearrangement of this principle produces a set of repulsion and attraction forces when a coil is allowed to alternate and produces thrust in the center piece. The same arrangement is used as a regenerative brake to recover energy.

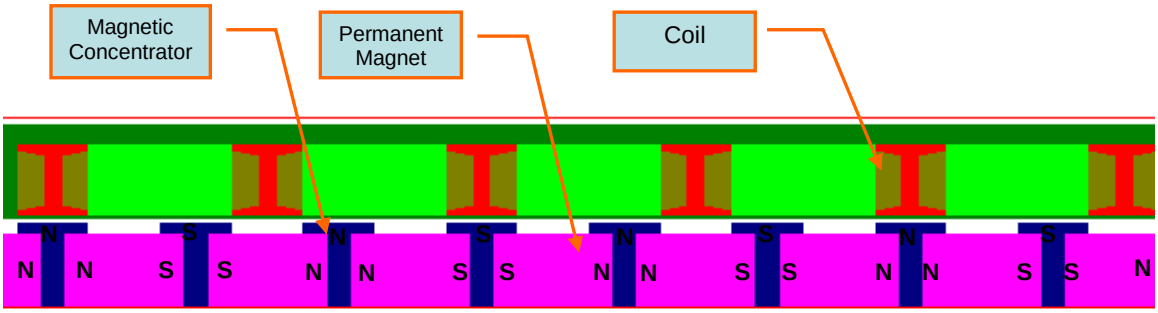

Figure 1.22: Berdut Linear Motor

1.4.1 Previous work

Several patents byBerdut describe prior work in this technology. They are series of publications based in the configuration shown in figure 1-7. Figure 1-23 shows a layout of those patents and their applications.

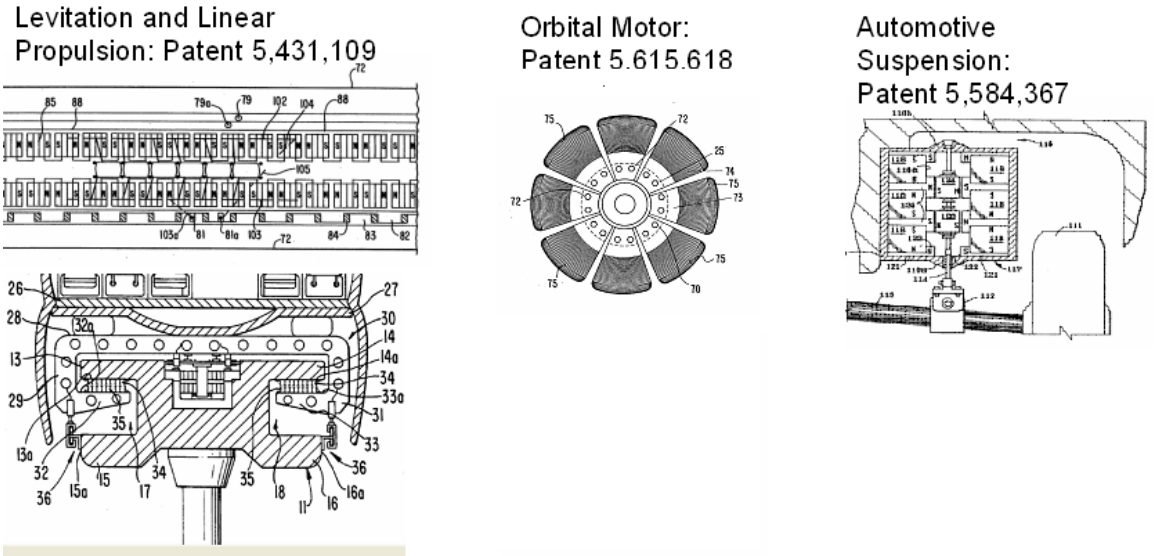

Figure 1.23: Different patents based in Berdut Technology and their applications

In addition, E. Medici and D. Serrano simulated the linear Berdut DC motor using a finite element method. Results were validated experimentally, showing an error of 6% in the thrust force. Figure 1-24 shows a general layout of the FE model employed in that research and figure 1-25 shows results for the thrust force. In the other simulation results, power and torque simulations resulted with error less than 6%, which are acceptable from an engineering point of view [2].

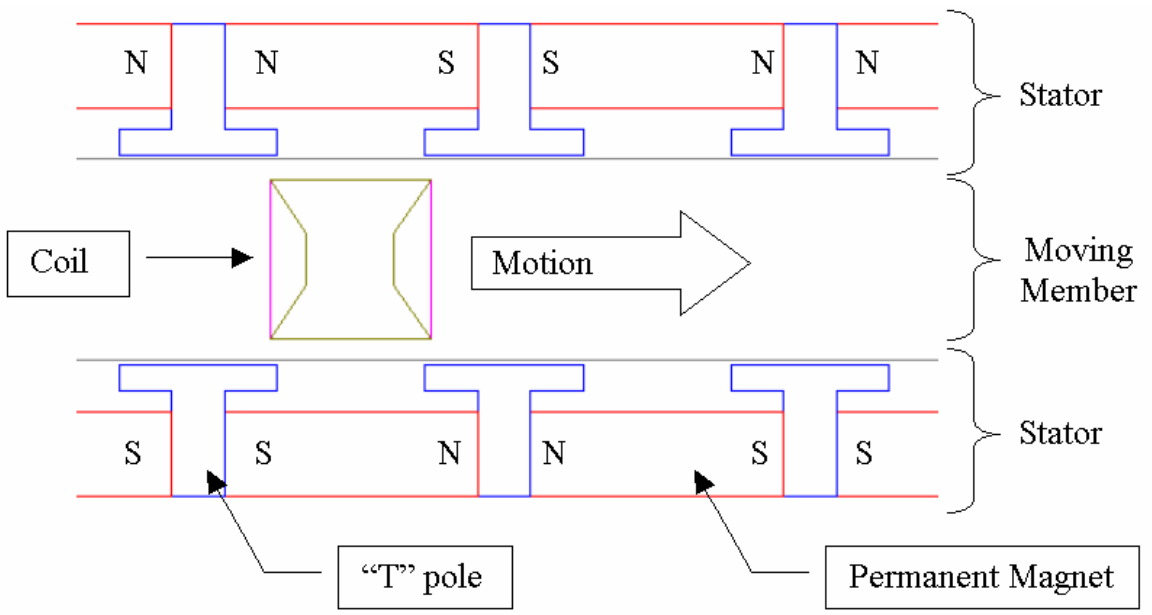

Figure 1.24: Layout of Berdut Linear Motor used by Medici and Serrano [2]

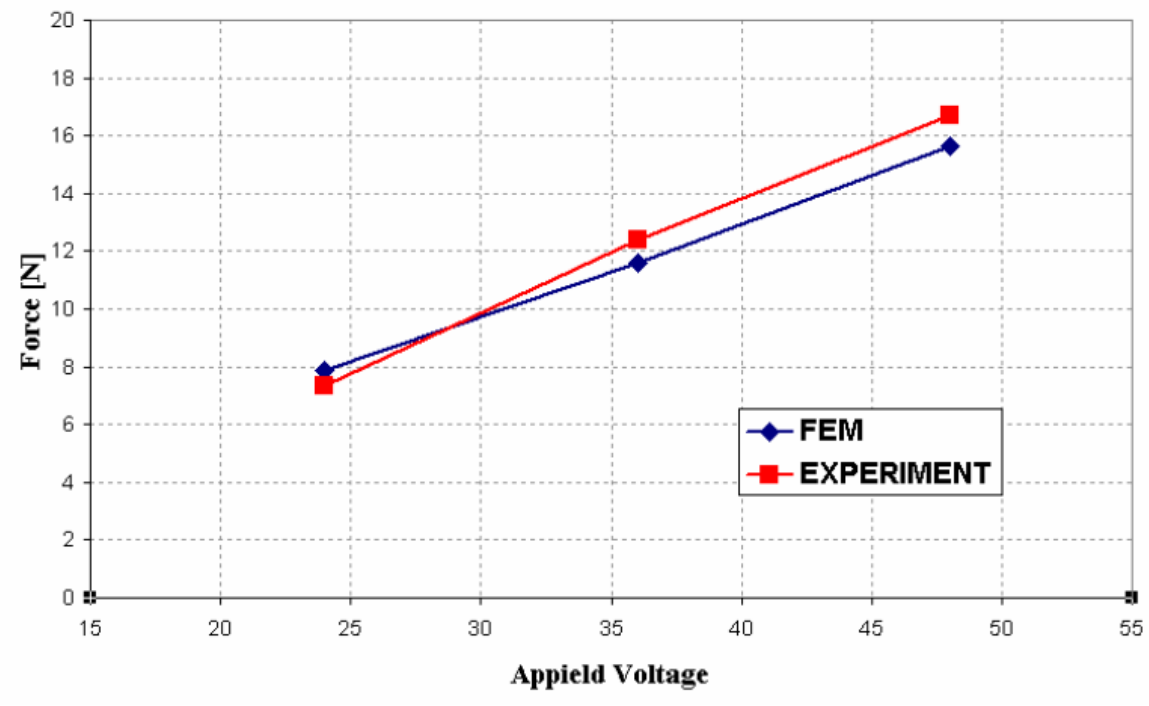

Figure 1.25: Thrust Force Comparison between simulated and experimental models made by Medici and Serrano [2]

2 THEORETICAL BACKGROUND

The operation of the Berdut linear DC motor is represented in figure 2-1. A coil with a current (I_{coil}) and a velocity ($\dot{x}$) produces a magnetic field (B) that interacts with a magnetic field generated by permanent magnets. The interaction between the current and the magnetic field generates a force but also power losses due to eddy currents and hysteresis. It is desired to calculate the Force (F) that will sustain a velocity ($\dot{x}$). Also it of interest to calculate the losses associated to that interaction.

The electric, magnetic and dynamic interaction in this motor is represented by a combination of the Maxwell's and Newton's equations, along with boundary conditions that setup their solution.

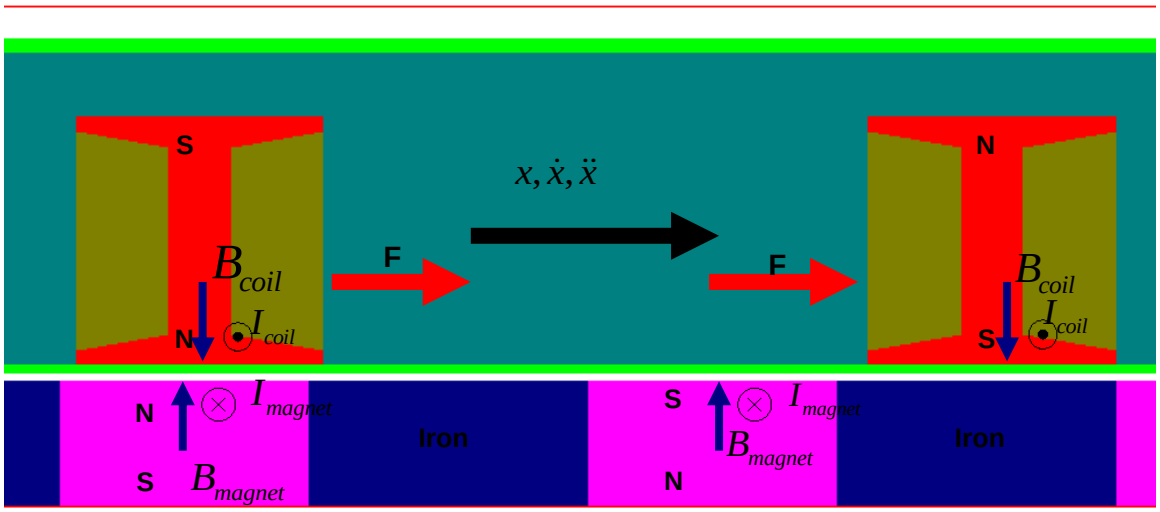

Figure 2.1 Berdut Motor Model

2.1 Governing Equations

The four Maxwell equations are: [1]

Magnetic Dipole

$$\nabla \cdot B = 0 \quad \textbf{(2.1)}$$

Gauss' Law

$$\nabla \cdot \varepsilon E = \rho \quad \textbf{(2.2)}$$

Faraday's Electromagnetic Induction Law

$$\nabla \times E = \frac{-\partial \mathbf{B}}{\partial t} \quad \textbf{(2.3)}$$

Modified Ampere's Law

$$\nabla \times H = J + \frac{\partial D}{\partial t} \quad (2.4)$$

In the above equations:

∇ = Del-operator

B = magnetic flux density

D = current displacement

ρ = charge density

E = electric field

H = magnetic field intensity

J = current density

t = time

All these equations come from experimental results. A brief explanation for each one follows.

For the first and second equation, it is important to define what means divergence. In physical terms, the divergence of a three dimensional vector field is the extent to which the vector field's flow behaves like a source or a sink at a given point.

The first equation comes from the fact that it is experimentally observed that in a magnetic field (B), that source or sink always form a closed loop. In that loop, the magnetic field lines are continuous; they do not begin or end as electric field lines do on charges. The magnetic field works in dipoles, traveling from the North to the South pole, i.e. needs both poles to exist. Figure 2-2 shows a magnet with its flux lines that demonstrates graphically this principle.

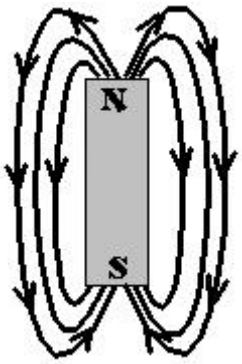

Figure 2.2: Magnet showing that always two poles are needed in order to form a magnetic field

The second one is Gauss's law, which establishes that the electric displacement in a closed surface is proportional to the electric charge enclosed by that surface. That displacement includes the contribution of free and polarized charges and it is a function of the electric field. When that field diverges, it is always equal to the sum of the charges inside the surface. Figure 2-3 shows a closed surface (S), in which an electric field (E) acts in an infinitesimal surface (da) in the direction of n. Also, there is a charge (q_i) at a distance (r_i) that represents the free charges mentioned above, acting in the dielectric volume. The relationship between the electric field and the free charges is [1]:

$$\oint_S (D \cdot n)\, da = \rho \Delta V \qquad \textbf{(2.5)}$$

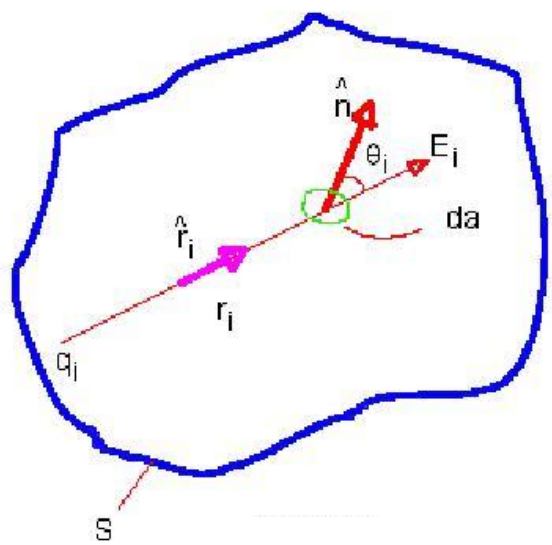

Figure 2.3: Interaction of the free charge and the electric field in a closed surface

Dividing by the differential in volume (dV), the differential Gauss law (equation 2.2) is established.

Equation 2-3 is Faraday's electromagnetic induction law, which is independent from the other experimental ones. It associates the electromotive force that is produced every time the magnetic field changes in a circuit. Figure 2-4 shows how that law works. The induced electric field is equal to the negative rate of change of the magnetic field. The negative sign comes from the Lenz law. It states that, when a magnetic field changes, (for example when moving with respect a conductive medium), the induced electric field produces currents. Then, those currents generate a magnetic field that opposes to the one that is moving.

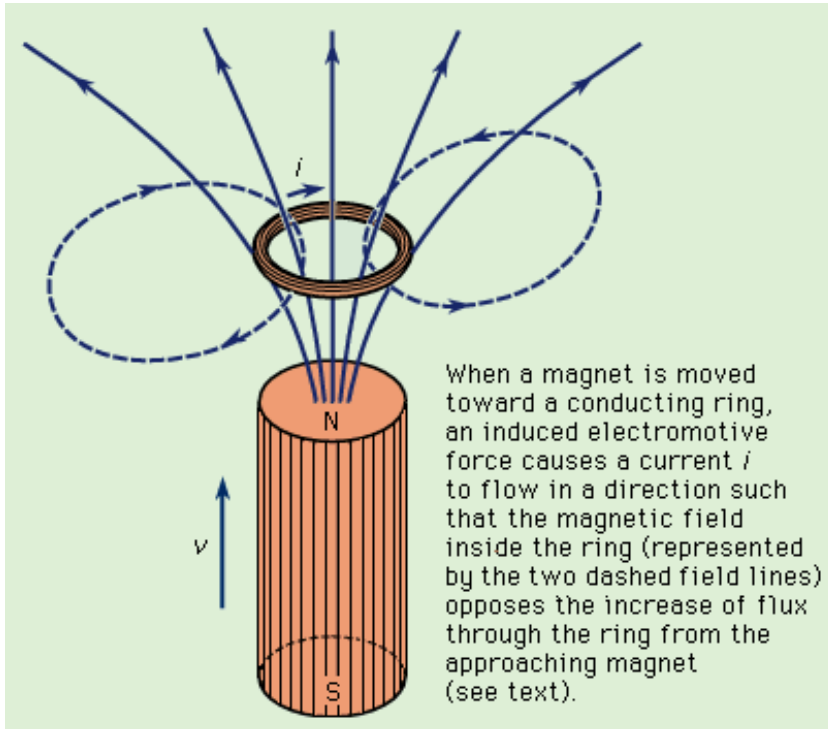

Figure 2.4: Induction between a moving magnet and coil

The last equation is the modified Ampere law. It is used to find the magnetic field due to the current delivered to a system (J) and for the rate of change of the current displacement $\left(\frac{\partial \mathrm{D}}{\partial t}\right)$, which was described in the Gauss law.

In addition, the constitutive equations are:

Electrical Displacement

$D = \varepsilon E$ **(2.6)**

Intrinsic to Normal Curve Relationship

$H = \frac{B}{\mu} - M$ **(2.7)**

Ohm's Law

$J = \sigma(E + \dot{x} \times B)$ **(2.8)**

Here, the variables mean:

ε = dielectric constant

μ = magnetic permeability

M = magnetization

σ = electrical conductivity

$\dot{x}$ = velocity

In all these equations, it is common to find at least one material property, such as ε, μ and σ.

The electric displacement comes from the Gauss' law and establishes the relationship between the electric field and the free and polarized charges. According to Gauss'law [1]:

$\oint_S E \cdot n da = \frac{1}{\varepsilon}\left(Q + Q_P\right)$ **(2.9)**

Where,

$$Q_P = -\oint_S P \cdot n da \quad \textbf{(2.10)}$$

Substituting 2-10 in 2-9, the free charge can be defined as:

$$Q = \oint_s \left(\varepsilon_0 E + P\right) \cdot n da \quad \textbf{(2.11)}$$

The term inside the integral parenthesis is defined as the electrical displacement:

$$D = \left(\varepsilon_0 E + P\right) = \left(\varepsilon_0 E + \chi E\right)$$

In the above term, ε_0 is the electric permitivity and χ is the electrical susceptibility. As in the case of the dielectric constant ε, ε_0 and χ are materials properties. Furthermore, these three variables are defined by:

$$\varepsilon = \varepsilon_0 + \chi$$

By regrouping terms in 2-12, the electrical displacement equation can be obtained.

The second constitutive equation deals with two curves: the intrinsic curve and the normal curve. Both of them are used in design of magnets. The first one relates the magnetization (M) with the magnetic field (H). The second one relates the induction (B) with the magnetic field intensity.

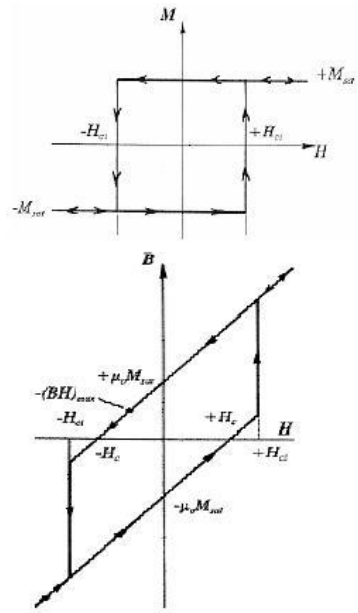

Equation 2-8 is Ohm's law which states that current density is produced due to an electric field and/or a magnetic field. They are related by a constant: the conductivity.

Substituting the terms of the magnetic field intensity and current displacement in Ampere's law (2-4) by the electrical displacement (2-6) and the Intrinsic to Normal curve relationship (2-7), results in:

$$\nabla \times B = \mu J + \mu \nabla \times M + \mu\varepsilon \frac{\partial E}{\partial t} \quad \textbf{(2.12)}$$

In the above equation, $\nabla \times M$ is the same as $J_{M,}$ known as the magnetization current. Also, the effect of the velocity of light is ignored due to the fact the application operation is well below that value. Therefore, the term $\mu\varepsilon = \frac{1}{c}$, where c is the light velocity is removed from 2-8, yielding to [2]:

$$\nabla \times B = \mu J + \mu \nabla \times M \quad \textbf{(2.13)}$$

Introducing the vector potential formulation, the magnetic flux density (B) can be expressed in terms of the vector potential (A) as:

$$B = \nabla \times A, \quad \textbf{(2.14)}$$

That potential comes from the fact that the rotation of the magnetic flux density is not zero. Furthermore, it satisfies the magnetic dipole, equation 2-1:

$$\nabla \cdot B = 0 \quad \textbf{(2.15)}$$

$$\nabla \cdot \left(\nabla \times A \right) = 0 \quad \textbf{(2.16)}$$

The divergence of a rotation is zero by mathematical definition; therefore equation 2-1 is satisfied.

Inserting 2-14 into 2-3 and rearranging leads to:

$$\nabla \times \left(E + \frac{\partial A}{\partial t} \right) = 0 \quad \textbf{(2.17)}$$

The vector denominated by the two terms inside the parenthesis has a curl equal to zero. Therefore, it is possible to obtain the electric field as a function of a scalar φ and the vector potential A [1]:

$$E = -grad\varphi - \frac{\partial A}{\partial t} \quad \textbf{(2.18)}$$

Substituting this equation into the Ohm's law (2-8) results in:

$$J = \sigma\left(-\frac{\partial A}{\partial t} - grad\varphi + \dot{x} \times \nabla \times A\right) \quad \textbf{(2.19)}$$

Then, this equation and 2-10 are used to rewrite 2-9 as an expression of vector potential [1], [4]:

$$\nabla \times (1/\mu) \nabla \times A = -\sigma \frac{\partial A}{\partial t} - \sigma grad\varphi + \sigma \dot{x} \times \nabla \times A + \nabla \times M + J_s \quad \textbf{(2.20)}$$

The meaning of every term here is as follows:

$\sigma \frac{\partial A}{\partial t}$ = Skin effect contribution. It is caused by eddy currents, produced when an AC current is distributed through a conductor. It is greater at the conductor surface than at the core.

$\sigma grad\varphi$ = Current passing through conductor to which is applied an electric field

$\sigma \dot{x} \times \nabla \times A$ = Induced current due to relative motion of a magnetic source with respect to a conductive material.

$\nabla \times M$ = Current due to magnetization. It is produced every time a conductor is subjected to a magnetic field.

J = External current source

In addition, an expression for the dynamic movement is needed to understand the behavior of a system such as the one presented in this thesis. Therefore, Newton's second law of motion is then used as:

$$m\ddot{x} + c\dot{x} + kx = F \quad \textbf{(2.21)}$$

In this equation, the parameters mean:

m = mass of the object that endures movement

c = damping coefficient

k = stiffness coefficient

$x, \dot{x}, \ddot{x}$ = displacement and its two first derivatives with respect to time: velocity and acceleration

F = applied external forces – This parameter combines forces electric, magnetic, gravitational, structural, thermal and drag forces. In this investigation, it was assumed that only the first two acts into the motor. They are represented by the Lorentz force:

$$F_l = \rho(E + \dot{x} \times B) \quad \textbf{(2.22)}$$

Using the Newton second law of motion, along with the Lorentz force equation yields to:

$$m\ddot{x} + c\dot{x} + kx = \rho(J \times \nabla \times A - grad\varphi) \quad \textbf{(2.23)}$$

The two sets of coupled equations that will solve the problem statement of figure 2-1 are:

$$\nabla \times (1/\mu) \nabla \times A = -\sigma \frac{\partial A}{\partial t} - \sigma grad\varphi + \sigma \dot{x} \times \nabla \times A + \nabla \times M + J_s \quad \textbf{(2.20)}$$

And,

$$m\ddot{x} + c\dot{x} + kx = \rho(J \times \nabla \times A - grad\varphi) \quad \textbf{(2.23)}$$

Equation 2-20 is a partial lineal differential equation, while 2-23 is an ordinary lineal differential equation. The primary objective is to solve simultaneously this set of coupled equations. The variables: $m, c, k, \rho, \mu, J_s, \sigma$ and M are known and the unknowns are: the vector potential $A(x, y, t)$, the scalar potential $\varphi(x, y, t)$ and the position $x(t)$.

In order to achieve the solution, boundary and initial conditions need be established. Among the different types of boundary and initial conditions that can be applied to Maxwell's equations are: Neumann, Drichlet and Balloon boundary conditions, [1, 5].

The Neumann, or natural boundary condition specifies that the normal component of the flux density (B) and the tangential component of the flux intensity (H) are continuous across the object surface:

$B_{1n} = B_{2n}$ **(2.24)**

$H_{1t} = H_{2t}$ **(2.25)**

A proof of equation 2.24 can be demonstrated using figure 2-5 and Maxwell's equation for magnetic dipole, equation 2-1. Figure 2-5 shows a control volume that has been set up in the interface of two surfaces, 1 and 2.

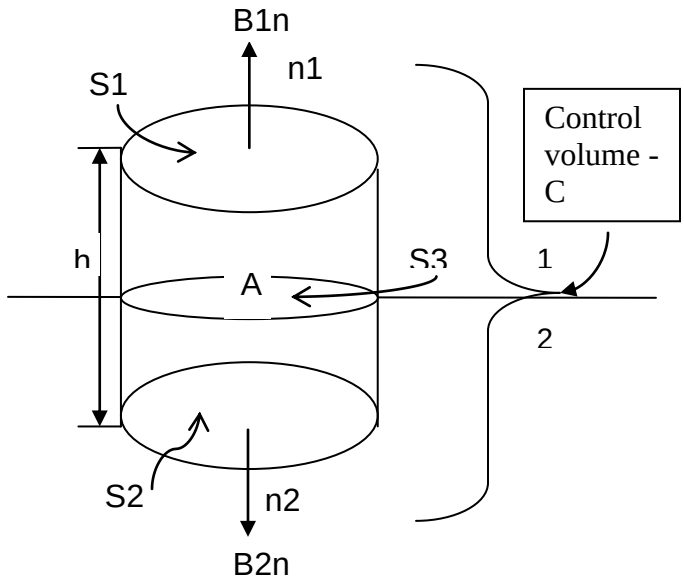

Figure 2.5 Control volume in the interface of two surfaces

In this figure:

C = control volume in the interface of two surfaces

S3 = surface that takes place in the interface

S1, S2 = surfaces that meet at S3

A = cross sectional area of the control volume

h = height of the cylinder

n1, n2 = unit vectors pointing away the interface

B1n, B2n = normal component of the flux density

Applying the divergence theorem, equation 2-1 to the control volume C, it is obtained the following expression:

$$\oiint_S (B \cdot n) da = \int_{S1} (B \cdot n_1)\, da + \int_{S2} (B \cdot n_2) da + \int_{S3} (B \cdot n_3)\, da = 0 \quad \textbf{(2.26)}$$

As the distance between S1 and S2 decreases, the last integral does the same until it reduces to zero. $\oiint_S (B \cdot n) da = \nabla \cdot B$, therefore, equation 2-26 reduces to:

$$\int_{S1} (B \cdot n_1)\, da = -\int_{S2} (B \cdot n_2) da \quad \textbf{(2.27)}$$

Due to the fact that n_1 and n_2 are opposite in direction, equation 2-24 is automatically satisfied.

This boundary condition is found when modeling symmetric or periodic geometry, as shown in figure 2-6 [5]. However, for this investigation the full motor was modeled and therefore it was not considered.

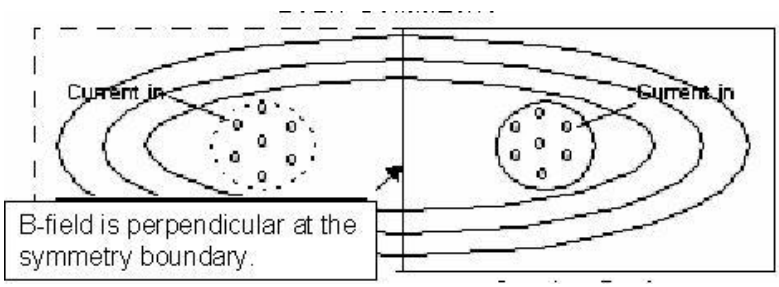

Figure 2.6: Boundary condition for the normal component of the magnetic flux density (B)

Equation 2.25 is obtained by integrating the fourth Maxwell equation in an area enclosed by a circuit. When that area tends to be zero, the resultant boundary condition is:

$H_{1t} - H_{2t} = j_{s\perp}$ **(2.28)**

The term at the right of this expression is the current density that runs perpendicular to the magnetic field intensity (H), which is a finite current along an infinitesimal surface. It is zero, excepting for infinite conductivity. Therefore, the right hand term in equation 2.28 is equal to zero and thus results in equation 2.25 results. It is also used to model symmetry and periodicity and therefore was not used in this investigation. Figure 2.7 shows how looks a boundary condition for the tangential component of the magnetic field intensity in the interface of two surfaces.

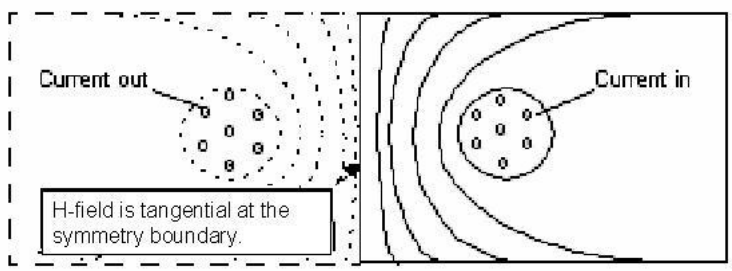

Figure 2.7: Boundary condition for the tangential component of the magnetic field intensity (H)

The second type of boundary conditions is known as Drichlet (or value). It forces the magnetic vector potential to become constant at the boundary and it is used to model the presence of a narrow conductive surface at the interface of two objects. That potential was defined in equation 2.14 as $B = \nabla \times A$. Assuming a two-dimensional magnetic field, a

constant vector potential in the z-direction only and rewriting A by its components, the following expression arises:

$$B = \frac{\partial A_z}{\partial y}\hat{i} - \frac{\partial A_z}{\partial x}\hat{j} \quad \textbf{(2.29)}$$

Therefore, if the boundary is horizontal, the partial derivative of x is zero, letting the magnetic flux density to have a component in the $\hat{i}$ direction only. The same reasoning applies to a vertical boundary, [5]. Thus, it can be concluded that B will be only tangential. Figure 2-8 shows this explanation for a value boundary condition in the vertical direction applied at the right edge. The magnetic flux density is parallel to this edge and points to the $\hat{j}$ direction only.

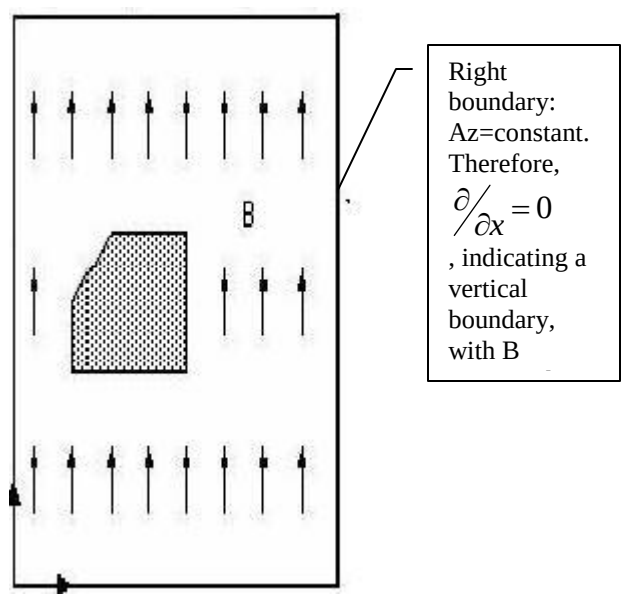

Figure 2.8: Drichlet boundary condition for constant Az in the vertical direction

The third condition deals with balloon boundaries. They are used to model the limits of the geometry, so it can be isolated from other fields. In this type of condition, the vector potential tends to be zero as the boundary goes to infinity. Mathematically, it is expressed as:

$$A_z \Big|_{\infty} = 0 \quad \textbf{(2.30)}$$

This boundary condition was used in this work. Figure 2-9 shows an area of the models investigated. The red rectangle is a balloon boundary condition. Due to A_z=0, it has been specified that the simulated environment ends there, with enough confidence that the error for not considering more space will not affect the solution.

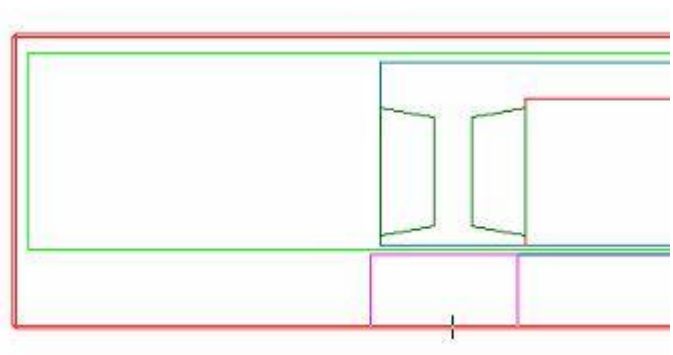

Figure 2.9: Balloon boundary condition represented by the red rectangle that surrounds this part of the geometry.

Regarding the magnetic field initial conditions, they are selected with respect to Maxwell's equations and the permanent magnets in use. For the dynamic part, the initial position and velocity are needed [2].

2.2 Numerical Analysis

Once equations 2-20 and 2-23 are solved for $A(x, y, t)$, $\varphi(x, y, t)$ and $x(t)$, according to their boundary conditions, it is needed to calculate the variables that will be used to solve the problem stated in figure 2-1.The equations that will be used are:

Magnetic flux density

$B = \nabla \times A$ **(2.14)**

Electric field

$E = -grad\varphi - \frac{\partial A}{\partial t}$ **(2.18)**

Velocity

$\dot{x} = dx/dt$ **(2.31)**

Force

$F_l = \rho(E + \dot{x} \times B)$ **(2.22)**

Losses

$\sigma \frac{\partial A}{\partial t}$ **(2.32)**

There is no closed solution for equations 2-20 and 2-23 but numerical methods may be used. Various alternatives are available but the Finite Element (FE) approach is more suitable to accommodate different geometries, no matter their shape and also has the advantage of including eddy currents into the field solution.

Because the scope of this research was to explore variations to the Berdut linear motor, programming was beyond the scope. Therefore, commercial software was selected to solve the numerical problem. That software used was Maxwell from Ansoft. Previous work by E. Medici [2] and J. Robles [3] validated the use of this software with experimental data. For example, figure 2.10(a) and 2.10(b) shows thrust force results from the finite element simulations and experiments that have 6% error in between.

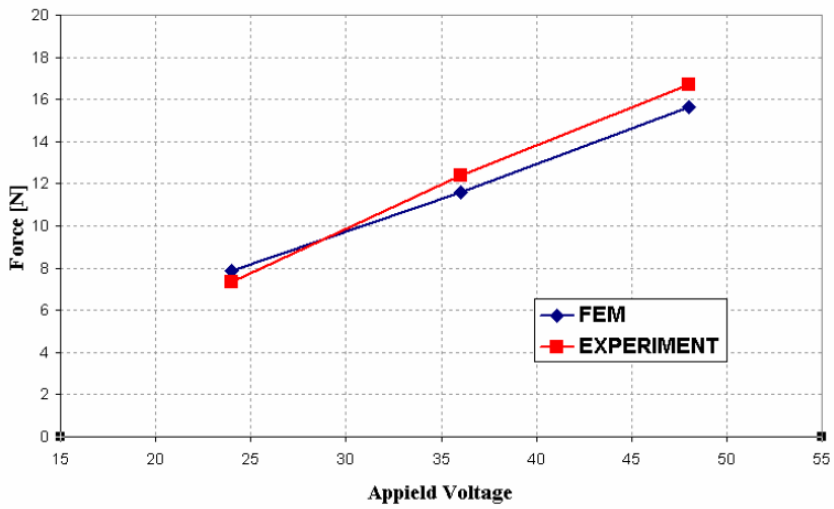

(a)

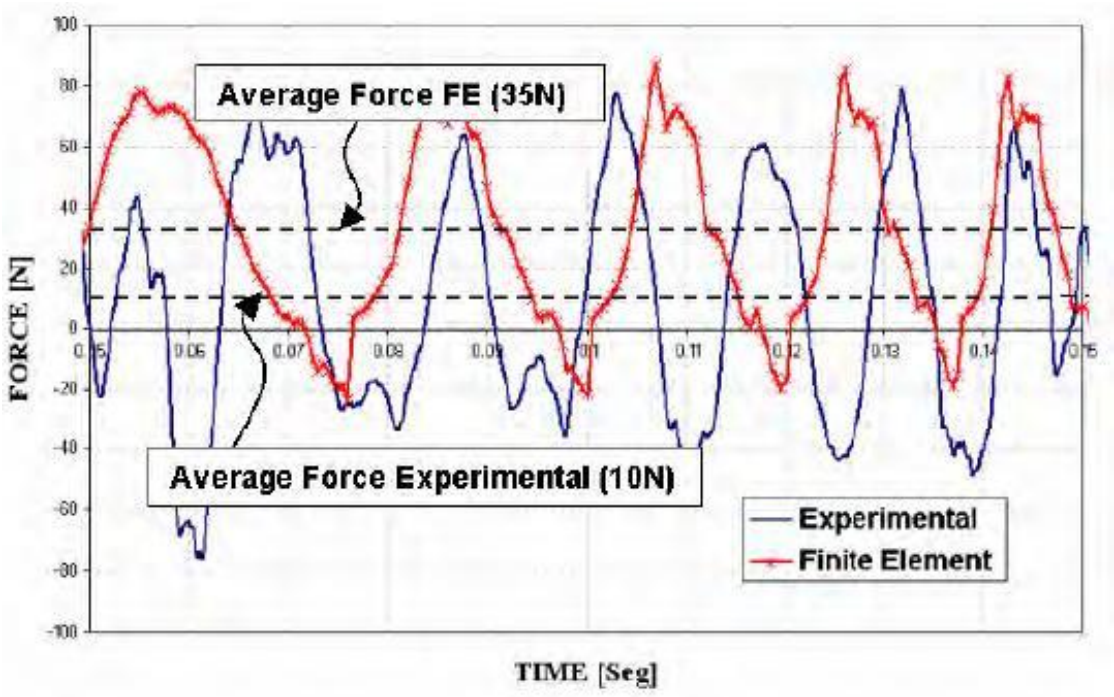

(b)

Figures 2.10 (a) and (b): Previous investigations show that Maxwell results are close to experiments

Maxwell uses triangular elements and linear interpolation functions to calculate the field solution. That function is called a polynomial weight function and is given by:

$$\psi_i := \frac{1}{2Ae}\cdot\left(\left(x_j y_k - x_k y_j\right) + \left(j_j - y_k\right)x + \left(x_k - x_j\right)y\right) \qquad \textbf{(2.33)}$$

Where,

Ae = area of the element

x_{ijk} = node coordinate of the element

x, y = any point within the element

It is important to notice that only x and y are used in the solution since the domain is 2-D only. Figure 2.11 shows the node locations in a triangular mesh created by Maxwell.

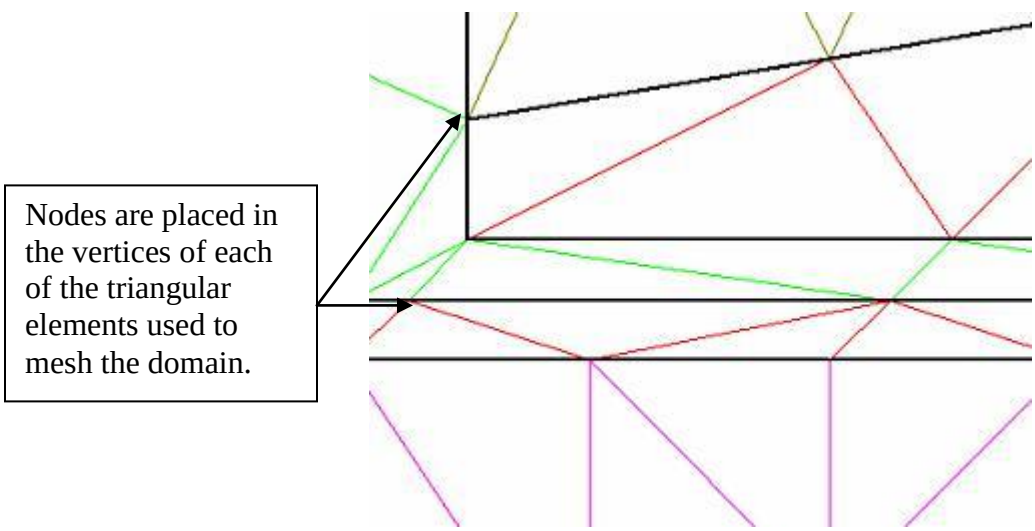

Figure 2.11: Close caption of the 2-D mesh made in Maxwell in which it can be appreciated the triangular elements and the node loacations

The vector potential is calculated as:

$$A^e\left(x,y,t\right)=\sum_{i=1}^{3}a^e\left(t\right)_i\psi_i\left(x,y\right) \qquad \textbf{(2.34)}$$

In this equation, a^e represents the approximation of the vector potential with respect to time and ψ_i is the weight function, equation 2.35. Substituting 2.34 in 2.35 and then into 2.20 allows to express the theoretical equations in terms of a first order, linear ordinary equation that can be solved numerically. That equation is:

$$\left[C\right]^e a^e\left(t\right)+\left[K\right]^e a^e\left(t\right)=\{J\}^e$$

In this equation:

$$\left[K\right]^e=(1/\mu)\int_\Omega\left(\nabla\times\psi^T\right)^T\left(\nabla\times\psi^T\right)dxdy-\sigma\int_\Omega\psi\left(\dot{x}\times\nabla\times\psi^T\right)dxdy+\sigma\int_\Omega\psi\left(\nabla\psi^T\right)(1/\mu)dxdy$$

$$\left[C\right]^e=\sigma\int_\Omega\psi\left(\nabla\psi^T\right)dxdy$$

$$\{J\}^e=\int_\Omega J_s\left(\psi^T\right)dxdy+\int_\Omega\left(\nabla\times\psi^T\right)^T H_c dxdy+\sigma\int_\Omega\psi\left(\nabla\psi^T\right)(1/\mu)dxdy$$

It is important to notice that physical properties σ and μ are kept constant during the solution. Also, the mesh will dictate where Newton's equation will be used and will be discussed in the FE Modeling section.

Once a solution for A(x,y,t) is obtained, the partial derivatives of A are calculated and used in equation 2.14 to find the magnetic field. They are:

$$\frac{\partial A^e}{\partial x} = \sum_{j=1}^{n} a_j^e \frac{\partial \psi_j^e}{\partial x} = \sum_{j=1}^{n} \frac{a_j^e}{2Ae}\left(y_j - y_k\right)$$
$$\frac{\partial A^e}{\partial y} = \sum_{j=1}^{n} a_j^e \frac{\partial \psi_j^e}{\partial y} = \sum_{j=1}^{n} \frac{a_j^e}{2Ae}\left(x_k - x_j\right) \quad \textbf{(2.35)}$$

2.3 Finite Element (FE) Modeling

This section describes how the model was setup in Maxwell. After the theoretical and numerical models were developed, a series of steps were followed in order to obtain from the software the desired output variables: F, $\dot{x}$ and the power losses, as described in figure 2-1.

These steps were:

1. Create the geometry and assign material properties.
2. Apply boundary and initial conditions, loads and analysis settings.
3. Mesh the model.
4. Solve
5. Post-process results

2.3.1 FE Modeling: Mesh

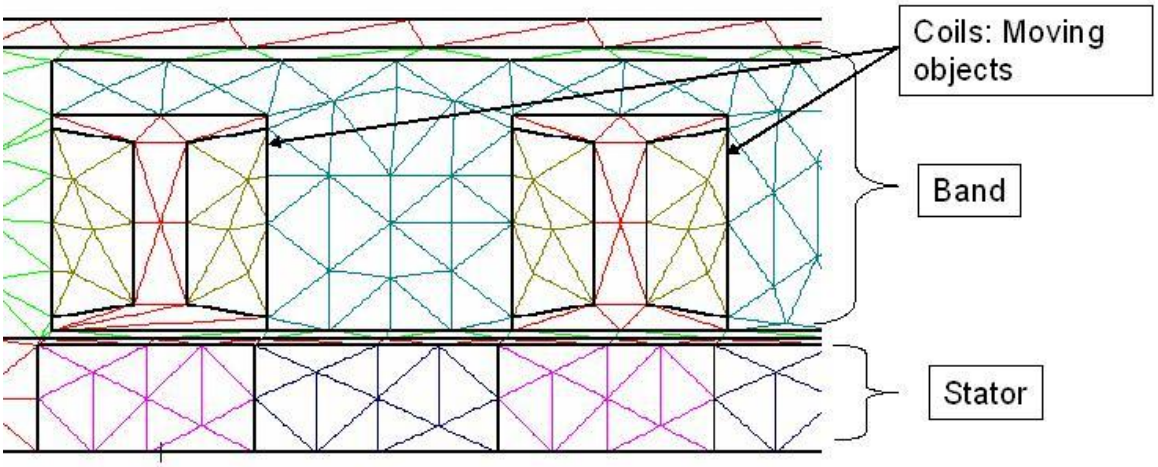

Figure 2.12 Principal Components of Mesh in a 2D Maxwell Model

Figure 2-12 shows the components of the mesh. It contains elements with a fixed size in the stator and the moving objects. Also, it contains the band, which is a section of the model in which all the moving objects are contained and that interacts with the stator elements by means of an adaptable mesh. In that type of mesh, the element geometry changes as the objects inside the band move along it. Figure 2-13 shows the mesh as the coil passes through the origin. In the top figure, the blue rectangle shows a fine mesh inside the band. In the figure at the bottom, it shows that this fine mesh has been moved along with the coils, leaving in the space behind it a coarser mesh. Inside the band, Newton's equation of motion calculates the position with respect to time, $x(t)$. Although no equation from theory was written in order to setup the solution, it is important to emphasize that the mesh will contain the approximate solution from the numerical method that is based in the theory.

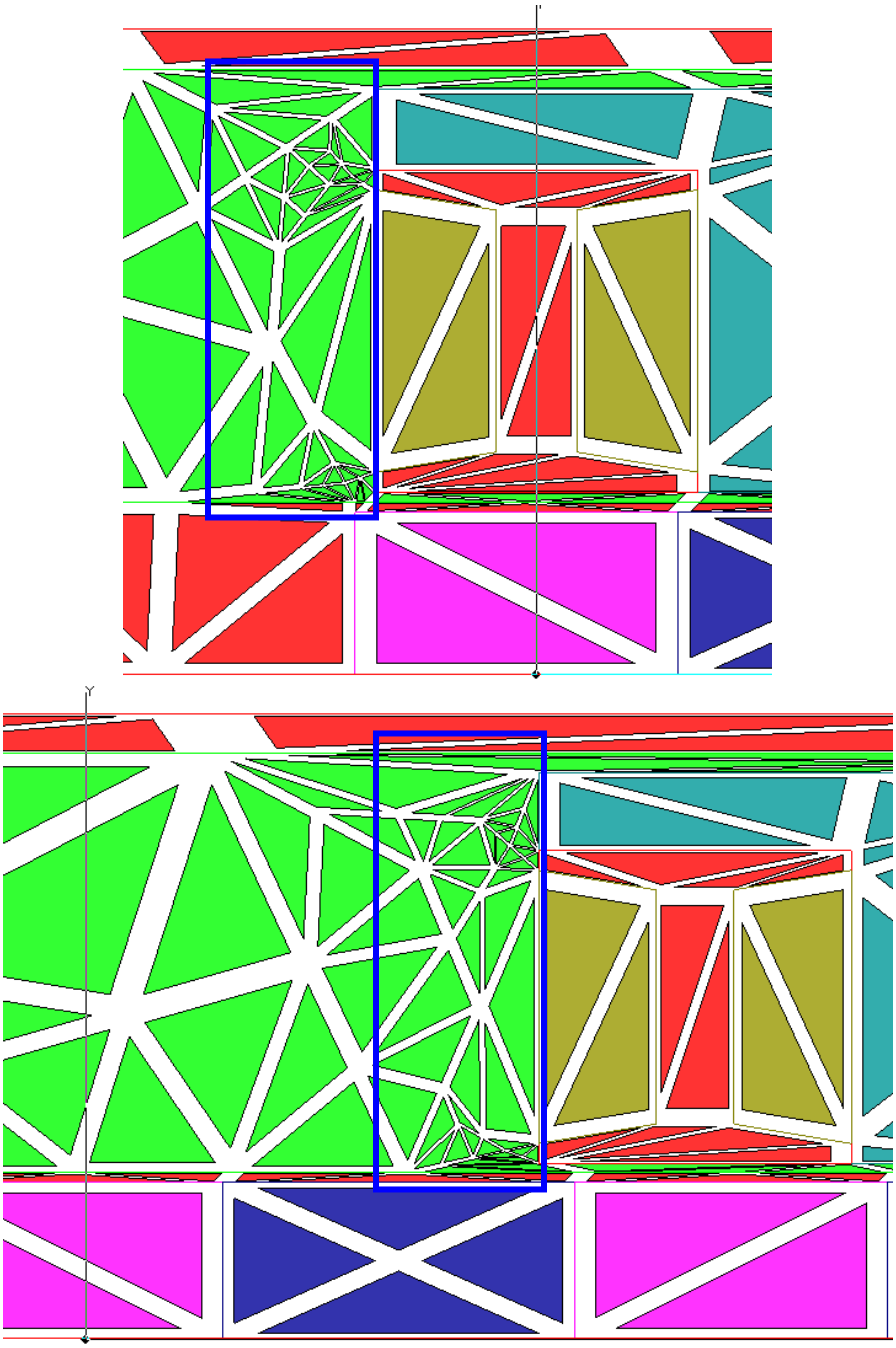

Figure 2.13: Changes in elements size at the band and between the band and the stator as the moving object passes through the origin.

2.3.2 FE Modeling: Sources of Power Loss

There are different ways in which input power is dissipated inside the motor. Two of them, caused by the eddy current and the hysteresis are due to the presence of the iron core. Also, friction is considered in brushed motors. The first two losses are described in this section.

The eddy currents are caused by the induced magnetic fields that produce an AC current that is distributed through a conductor. An expression for the power lost by these eddy currents is [6]:

$$P_e = K_e \sigma \omega^2 B^2 \quad \textbf{(2.36)}$$

In this equation, K_e is a constant that depends on geometry, σ is the electric conductivity, ω is the electromagnetic field frequency and B is the magnetic flux density. As these currents increase, more power is dissipated and therefore the motor is less efficient. Hence, a technique is commonly used to reduce the core conductivity. Instead of having a solid core, it is made by layers. The conductivity of this modified core is calculated as [12]:

$$\sigma_{eff} = \frac{\sigma SF}{N^2} \quad \textbf{(2.37)}$$

The variables σ_{eff}, SF and N are known as the effective conductivity, the stack factor and the number of laminations, respectively.

The energy lost due to the magnetization and demagnetization is called hysteresis. There are different factors that contribute to it such as: impurities, imperfections in the crystalline structure and cavities. Those factors make harder to align the domain in the direction of the applied magnetic field, i.e. to magnetize the material. Figure 2-13 at the left shows how domains are aligned after an external magnetic field is applied to the material.

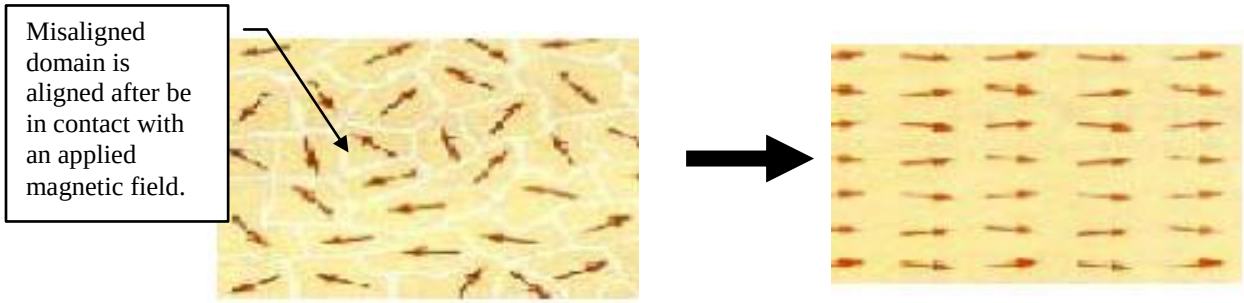

Figure 2.14: Magnetization Process

Figure 2-14 shows a hysteresis loop for typical ferromagnetic material, which is used to demonstrate the different steps in the magnetization-demagnetization cycle. In step 1-2, the material is magnetized at the first time. Then, at point 2, the magnetic field intensity is released and it starts to demagnetize by following step 2-3, until it reaches zero. At this point (3), there is still a magnetic flux density in the material which is called a remnant flux density. The remnant flux density makes permanent magnets possible because an external magnetic field is not needed to maintain them and produce magnetic induction. Hence, it can be concluded that another factor that contributes to hysteresis losses is the operation itself of the magnet [3, 7].

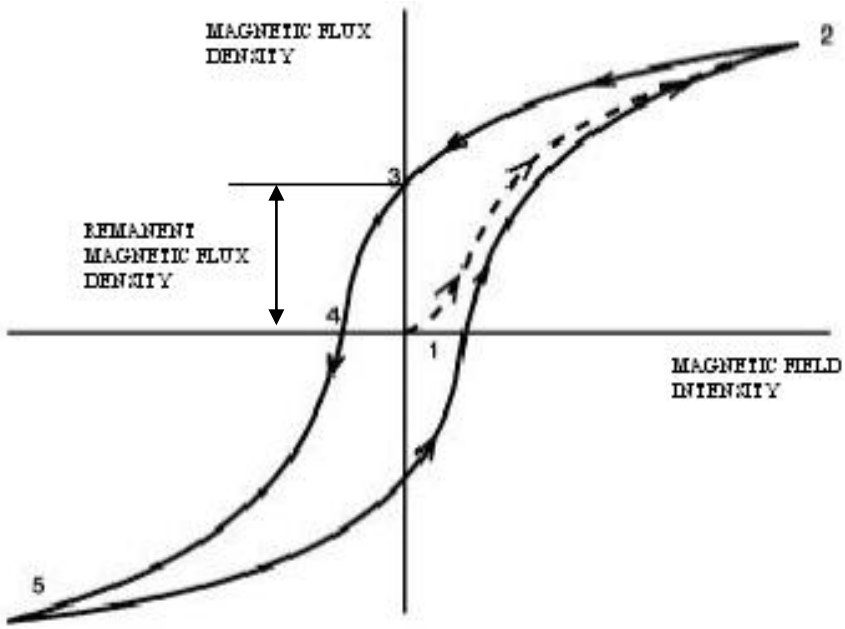

Figure 2.15: Hysteresis loop

The total energy lost is the area inside this loop. The power losses can be computed numerically by [6]:

$$P_L = K_L \omega B^n \qquad \textbf{(2.38)}$$

In this equation, ω is the frequency of operation, B is the magnetic flux density, n is the Steinmetz exponent and K_L is a constant that varies depending on the materials. For the exponent value, it is found to be 1.6 for iron cores. On the other hand, K_L is generally 0.001 for steels with silicon and ranges from 0.002 to 0.004 in soft steels [2, 13].

A curve such as Figure 2-16 is generated for linear materials, as well as for non-linear ones when operating in a small range. Important parameters in plots of these types are:

1. The coercitivity (H_c) – Magnetic field intensity when the magnetic flux density is zero.

2. The retentivity (B_r) – Magnetic flux density when the field intensity is zero.

3. Relative permeability (μ_0) – slope of the graph

Only two of these three properties are required to set up this graph. This model is used in the software to describe the materials properties.

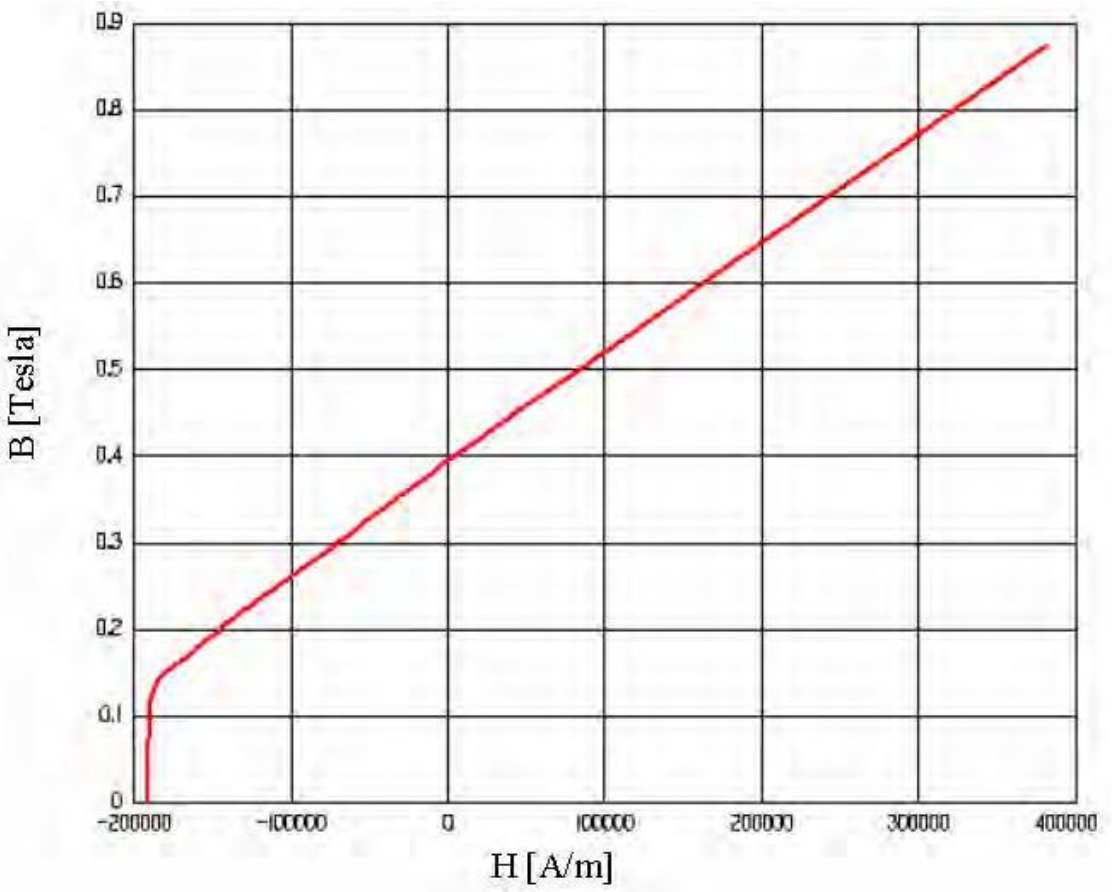

Figure 2.16: Hysteresis loop for Ceramic 5, a material used for permanent magnets

2.3.3 FE Modeling: General Model Dimensions

Figure 2-17 shows a diagram of the Berdut linear DC motor with the general dimensions and components. This arrangement is a variation of an orbital motor with two plates, a linear motor with equivalent design is the first variation to be studied. The base model is shown in figure 1.22 at the introduction.

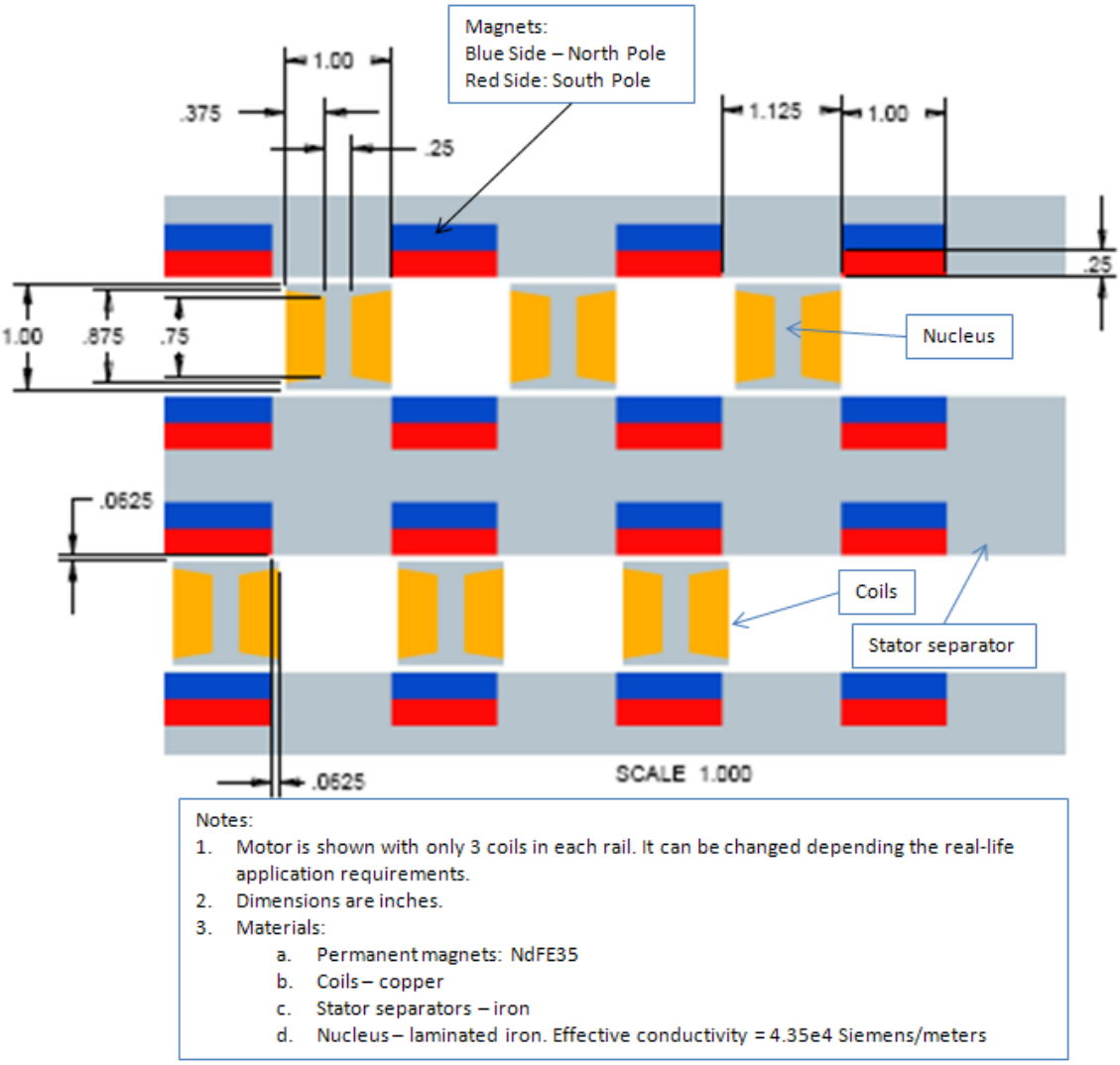

Figure 2.17: Berdut linear motor diagram with two rails. It shows the topology of the active-passive configuration.

The model shown in figure 2-17 has two switching cycles running in parallel. The one at the top is not electrified when the coils are approaching the magnets and is known as the passive cycle. On the other hand, the active cycle, at the bottom, uses a current to create

an electromagnet that repels the permanent magnet pole and is attracted by the iron next to it.

There are important notes about the drawing shown in figure 2-17:

- Motor is shown with only 3 coils in each rail. The real-life application can be made of any other number of coils. That depends on the requirements.
- Dimensions are in inches.
- Materials:
  - Permanent Magnets: NdFe3
  - Coils: copper
  - Stator Separators: iron
  - Nucleus: Laminated iron. SF=0.95 and N=15 for the effective conductivity at the nucleus. Effective conductivity =4.35e4 Siemens /meters

In addition, the following assumptions were made in order to construct the FE models for different configurations:

- The two rails run at the same velocity and therefore can be consolidated in one model. Also, the two rails should be consolidated because Maxwell allows only one band. The transition from two rails to one rail was made taking into consideration the relative dimensions in the two rails model.
- The mass is 1000 kg. It assumes a 454 kg car and 546 kg of passengers.

- The motor will always contain six coils in order to compare different configurations.
- Due to that comparison, only one portion (1.4 m) of the total length was modeled for all cases.

The simplified model is shown below:

Figure 2.18: Simplified model of the Berdut DC Linear Motor in which two rails were consolidated in one

The last assumption made is that the motor will be analyzed as if mounted on a dynamometer. Therefore, given a velocity, a load force was applied to counteract its effect. Furthermore, the velocity will keep constant throughout all the analysis. At the end of the simulation, it will drop to 0 m/sec because it reaches the translation limits; therefore it stops after reaching that position. Please refer to the model settings for a more complete explanation of these limits. The power output $\left(P_{output}\right)$ will be the final velocity $\left(\dot{x}\right)$ multiplied by the load force $\left(F_{Load}\right)$. In order to obtain the input power $\left(P_{input}\right)$, power losses $\left(P_{Loss}\right)$ should be added. They are calculated by the software. Finally, the efficiency $\left(\eta\right)$ is calculated as [2]:

$$\eta = \frac{P_{output}}{P_{input}} = \frac{F_{Load} * \dot{x}}{F_{Load} * \dot{x} + P_{Losses}} \quad \textbf{(2.39)}$$

2.3.4 Boundary Conditions and Sources

As pointed in the theory, Maxwell's and Newton's equations should be solved along with boundary conditions. The only boundary condition used in the model was the balloon condition. Figure 2-19 shows the model with this boundary condition applied.

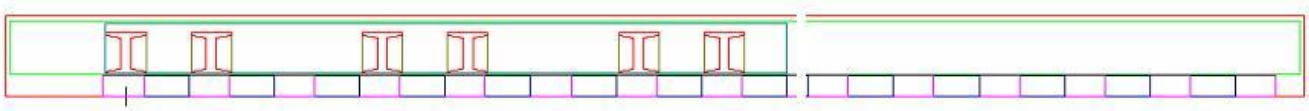

Figure 2.19: Balloon Boundary Condition. It is identified by the red rectangle surrounding the model.

The source applied to this model was an electric current. It is the current J_s that appears in equation 2.20. All the configurations studied in this research have a current source that is applied with the intent of reducing the power consumption and therefore increase the efficiency. Figure 2.20 shows a plot of this current and how it is applied to a single coil as it moves along the stator. Also, it shows the values of the input current, which were 24A (alternating between positive and negative) and 0A. Maxwell allows the user to select several inputs of current: constant, sinusoidal or user-defined. Also, the current can be a function of time, position or speed. Determining the time at which the coil will switch will add more complexity to this dual cycling. Therefore, the current was input as a

function of position using a user-defined square curve. The current changes as a function of position with respect to the magnets.

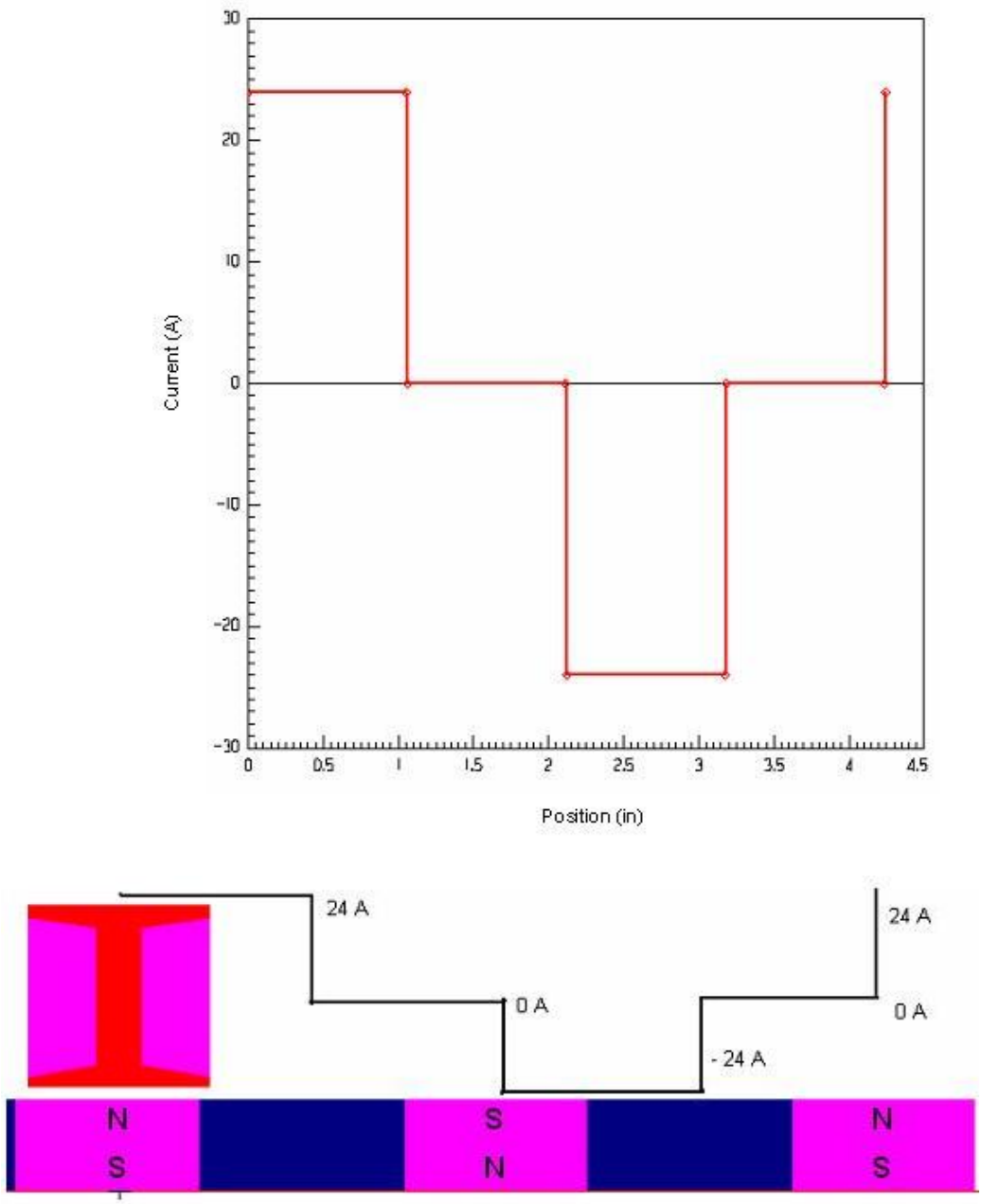

Figure 2.20: Switching in Berdut DC Linear Motor

2.3.5 Analysis Settings

The Berdut motor was analyzed using transient simulations. In order to perform them, Maxwell software needs several inputs in its setup. They are:

1. Mechanical setup – This input consists in the initial velocity, mass, damping coefficient and load force applied to the model. They are dependent on the application. In this case, it was assumed the train is traveling at different constant speeds of 3.6, 50 and 93.6 km/h and that it has been setup accordingly to accelerate until that speed. The mass was the sum of the car and the passengers, equaling 1000 kg. No damping coefficient will be considered due to the fact mentioned previously it has no effect [2].
2. Simulation end time and time step – The simulation end time is calculated as the positive translation limit divided by the initial velocity. The time step was taken to be $1/20^{th}$ of the total simulation time. A sensitivity study was performed in the selection of the time step.
3. Mesh definition – The default, current mesh setup from the program was assumed initially and a sensitivity study was performed in order to select a feasible mesh taking various tradeoffs into account such as convergence and CPU time.
4. Translation limits and model size – They are dependent on the model length. The application of interest will have a length of 0.5 km. However, for practical purposes and due to the cyclic symmetric properties, the translation limits extend

for only 0.8 meters. The model was 1.4 meters, as the software needs additional space after the imposed limits in order to work.

For other setup parameters, such as the type of solver used by Maxwell or residual value, a reference from previous work models was consulted and due to their success against experimental results, they were applied to the models in this investigation [2]. It was let to the software to select automatically the type of solver from the follwing two: Incomplete Conjugate Gradient (ICCG) or Direct. The difference between them is that the Direct always converge but is slower than the ICCG. On the other hand, the ICCG is faster but fails to converge in problems such as high premeabilites and small air-gaps [5]. Therefore, it can be concluded that the number of elements is less than 1500, as the case of the models presented here, the direct solver is used. The residual, which indicates how close a field solution satisfies the Maxwell equations was 1e-5.

3 BERDUT MOTOR SIMULATIONS RESULTS

As stated in the objectives, this investigation focuses in the assessment of the performance of different topologies based on the Berdut technology. A numerical model was made using the theory from Chapter 2 as a basis. That model takes as a reference point the configuration presented in Figure 1.22, which has been extensively investigated in previous works [2].

3.1 Configurations to be studied

An explanation of the different models assessed in this research follows. In the caption under the figure will be the name used when comparing results.

3.1.1 Berdut Classic Pole

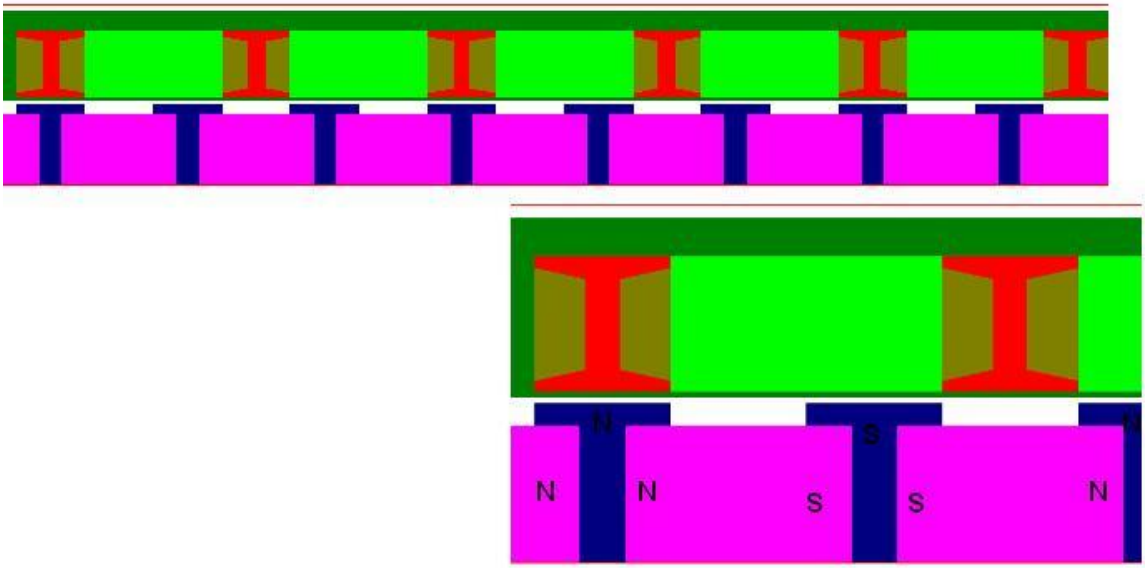

Figure 3.1: Original Configuration

This model uses the Berdut pole, with the T concentrator pole and it is the base configuration that has been studied previously. The model used in this arrangement contains one set of rails as shown in Figure 3.1. Coils are equally spaced as well as magnets, with a distance between centers of 38.1 mm. The switching energizes the first coil energized while the second one was inert. When the second coil is over the next pole it is energized and the first pole becomes inert. This pattern repeats switching. The material for the permanent magnets was NdFeB.

3.1.2 Out-of-phase switching: Two rails coupled in one

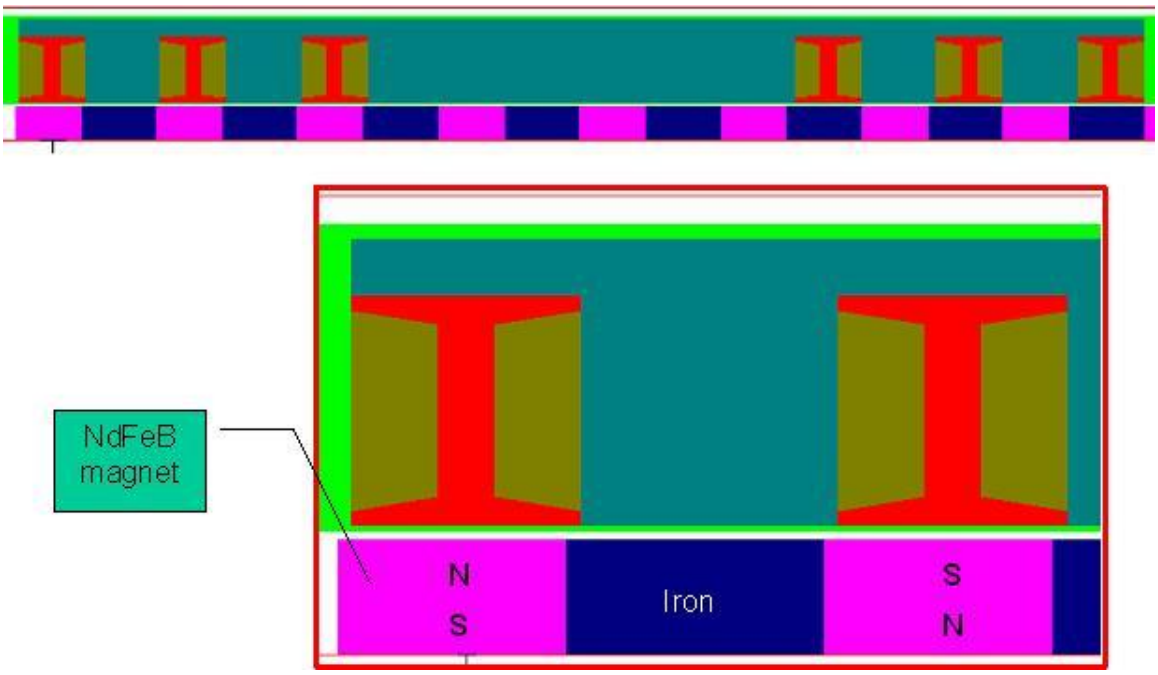

Figure 3.2: Coupled configuration

In this topology there are two sets of coils. The first three at the left are 1.5875 mm to the right of the permanent magnet centerline. At this point, they are energized, while the three at the far right are not. Once the first ones reach the right side of the iron at their right, they turn off. The other set, which is now 1.5875mm at the right of the permanent magnet centerline, delivers current. This cycling continues throughout all the length of the stator. Furthermore, it is the same switching as that in section 3.3.1: for any position three coils are active while three are inert. The space in between was made to prevent any interaction between the magnetic fields generated by those sets. In real life they run in separate rails, hence a realistic modeling should avoid flux lines to cross from one set to

another. Figure 3-3 shows an example for t = 0.021 sec. Any flux line from the electrified coil pass through the magnet at the immediate right (**M1**). The same behavior occurs in the inert coil, using the magnet just to its left (**M2**). Having another magnet at the center of the separation (**M3**) makes the flux from **M1** and **M2** pass through it, completing the magnetic loop. Therefore, no energy will pass directly from one set of coils to the other.

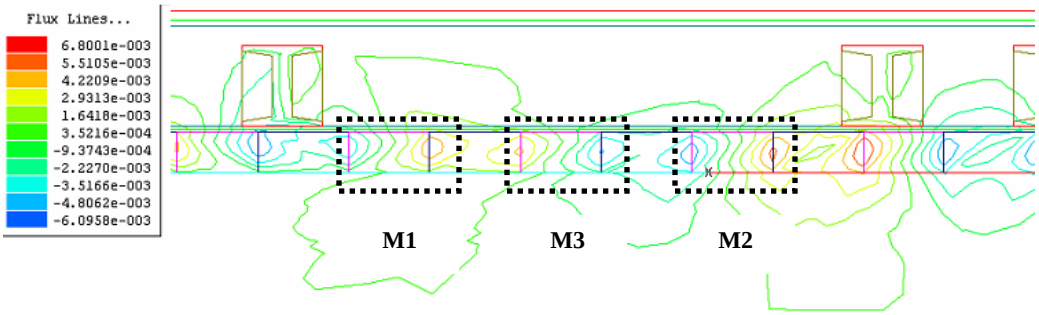

Figure 3.3: Space in between electrified and inert coils in out-of-phase configuration. It is made to prevent interaction between the two sets of coils.

3.1.3 In phase switching: Coils positioned to turn on at the same time

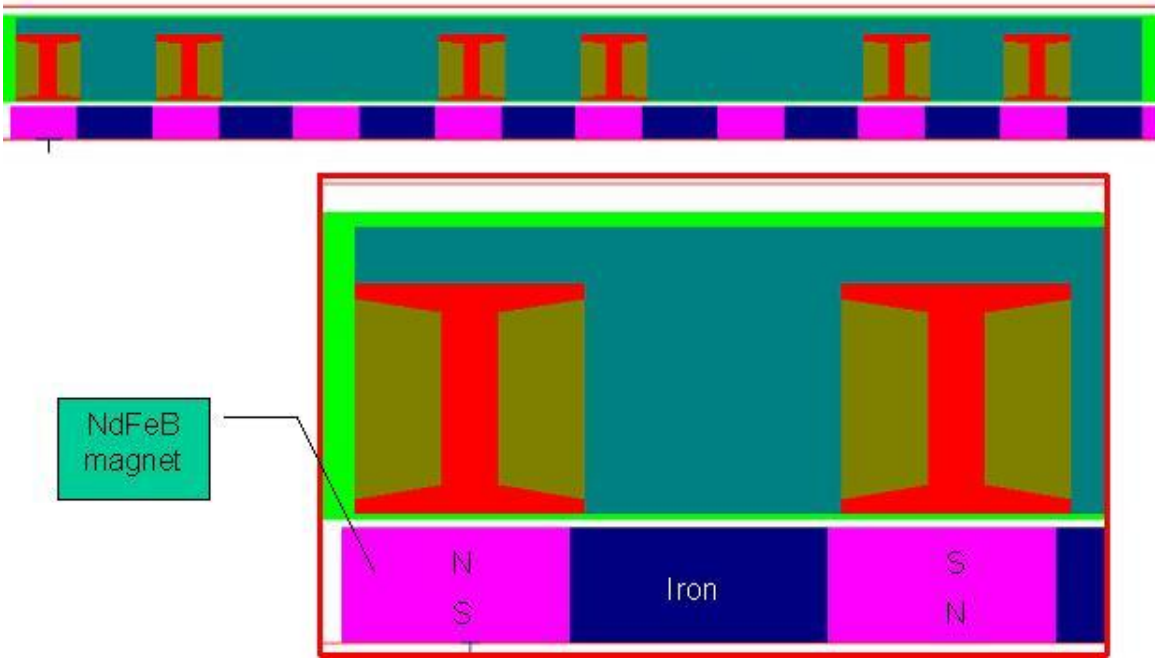

Figure 3.4: All-on

In this configuration, the six coils have an initial position of 1.5875 mm to the right of the permanent magnet centerline. Hence, the same input signal is used for all the coils simultaneously. That means the active and passive cycles always occur at the same time. This is the same principle of operation of a conventional linear motor, except for the turning off of the coils during part of the travel.

3.1.4 Out-of-phase and In-phase switching without irons

Currently, the Berdut motor contains iron-based material in between the permanent magnets. Their intended objective is to increase the force during the passive cycle. However, if the switching is not made at the best location, it is possible that the iron retracts the acceleration as it will want to attract the coil and not repel it. The following two models contain the same principle as the Out-of-phase and In-phase switching configurations shown in sections 3.1.2 and 3.1.3 with the exception they don't have the irons in the stator.

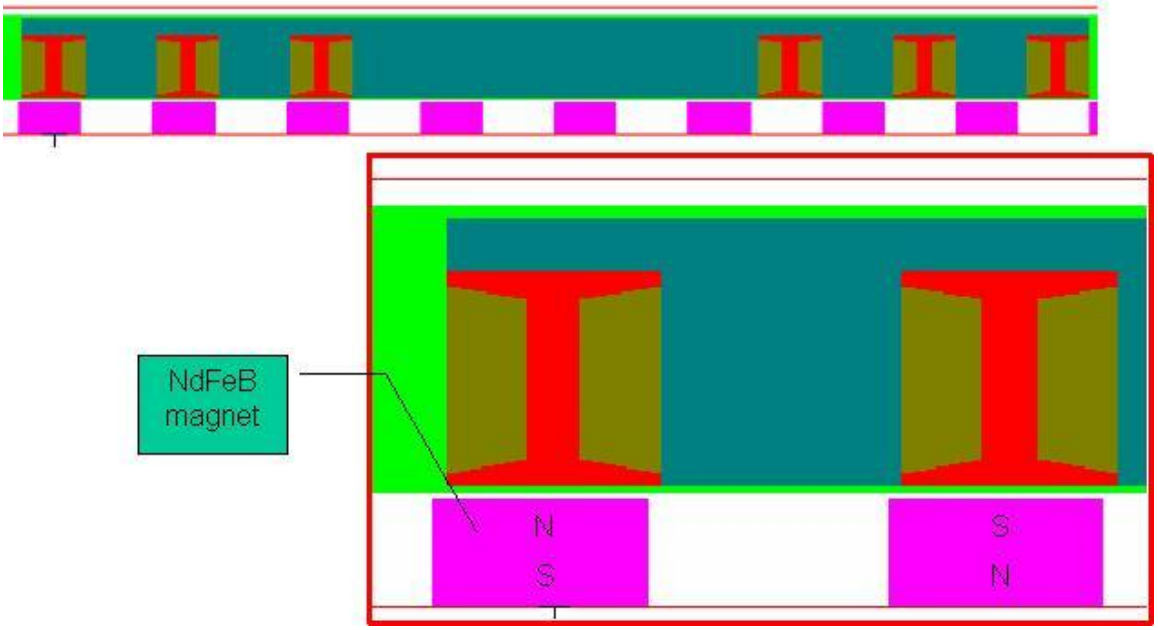

Figure 3.5: Coupled-no-irons configuration

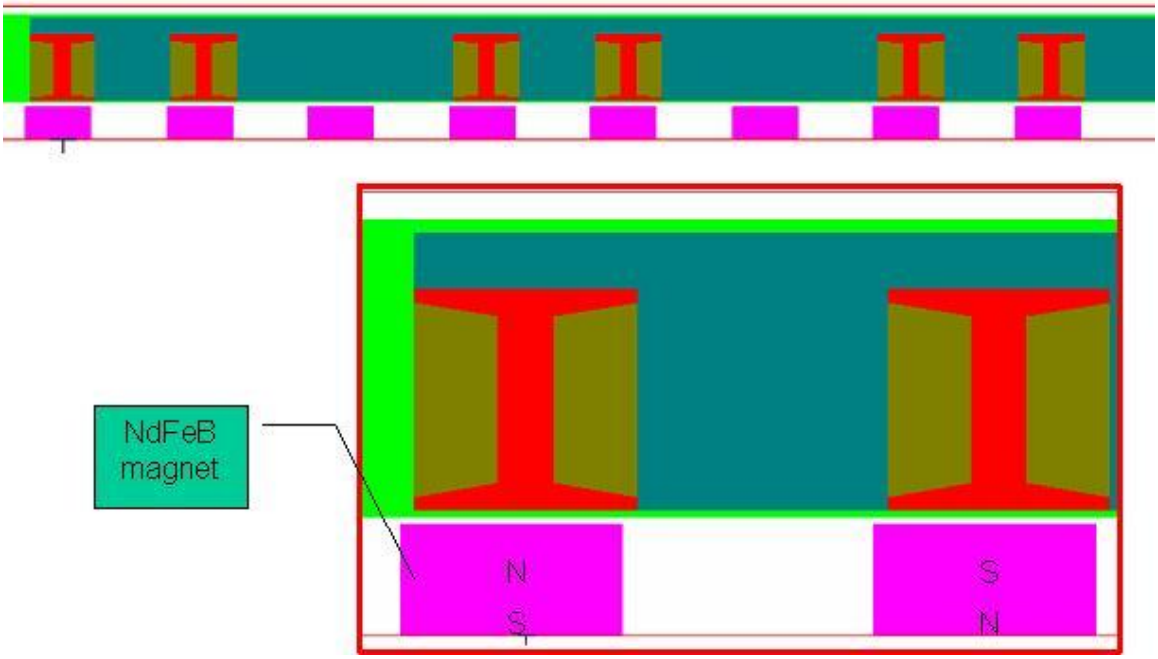

Figure 3.6: All-on_no_irons configuration

3.1.5 One rail with one common nucleus

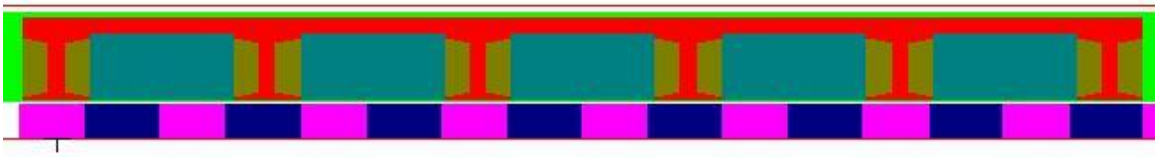

Figure 3.7: 1rail-common-nuc. Configuration

This configuration uses standard magnet poles of NdFeB with one iron at each side. As an innovative option for applications with magnets in one side only, the coils at the secondary part have a common laminated nucleus with the intent of concentrating the magnetic field. The coils turn on alternatively. First, third and fifth coils are electrified when their center pass 1/16” by the center of the magnet. In that position, second, fourth

and sixth are turned off. When the right edge of the first, third and fifth coil passes by the right edge of the iron in front of them, they turn off and the others three become switch on.

3.1.6 One rail, separated nucleus

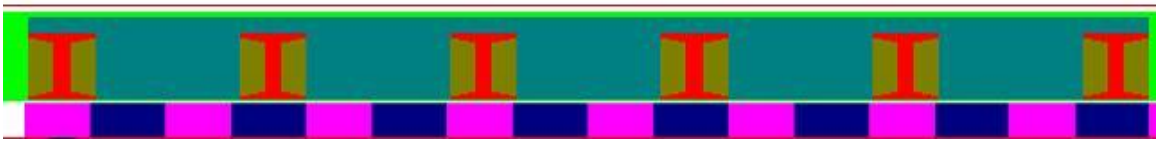

Figure 3.8: 1rail-sep-nuc. configuration

This model uses standard magnet poles of NdFeB with one iron at each side. It is an option for applications with magnets in one side only. However, the coils at the secondary part do not share a common laminated nucleus. This option was studied as an alternative of the **1rail-common-nuc** that offers simplicity. The coils turn on alternatively. First, third and fifth coils are electrified when their center pass 1/16" by the center of the magnet. In that position, second, fourth and sixth are turned off. When the right edge of the first, third and fifth coil passes by the right edge of the iron in front of them, they turn off and the others three become electrified.

3.2 Preliminary Analysis

In order to run the models with the best settings of time step and meshing, a sensitivity study was made to determine the impact of different time step values and took into

account the tradeoff between accuracy, CPU time and convergence. Results are as follows:

3.2.1 Time step

Two configurations were solved with different time steps. Then, efficiency was computed and the percent of error was compared within the models at different time steps. The initial time step was 1/20th of the simulation end time. Then, it was decreased to 1/200th and to 1/600th the simulation end time. Results show that the difference is more than 5% between the initial time step and the first decrease of the time step and less than 5% in the second decrease. Therefore, it was concluded that a suitable time step was **1/200th** of the simulation end time.

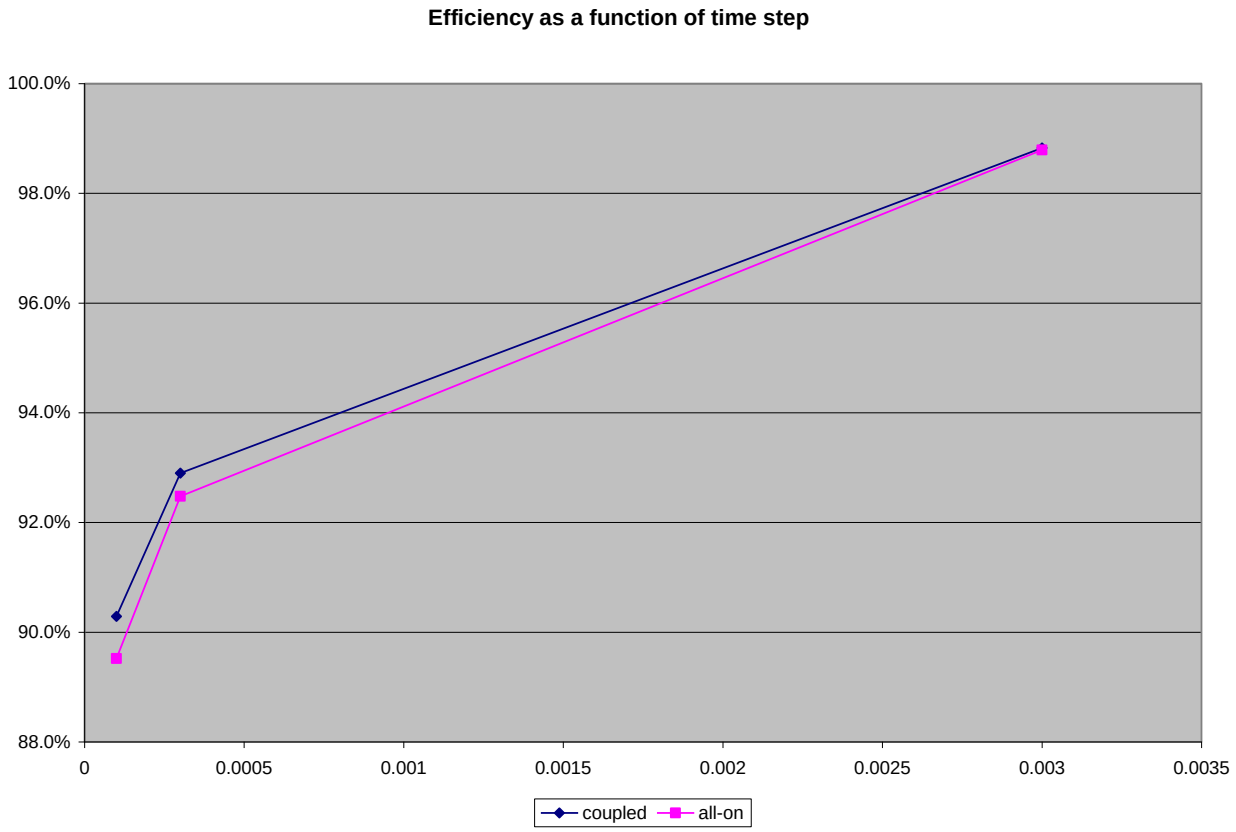

Figure 3.9: Effect of time step in efficiency results for two different configurations

3.2.2 Mesh density

Two configurations were solved with three different numbers of elements. Then, efficiency was computed and the percent of error was compared within the models at different number of elements It was concluded that the coarse mesh density, as shown in figure 3.10, is suitable to run the models of this investigation, as the results varied less than 5%. Figure 3.11 and the coarse mesh allowed for faster simulation execution times. Because all cases were run at the same mesh density, the results were compared.

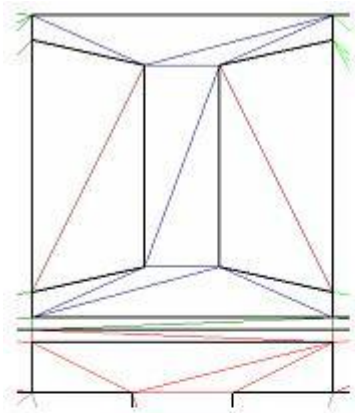

Core Mesh

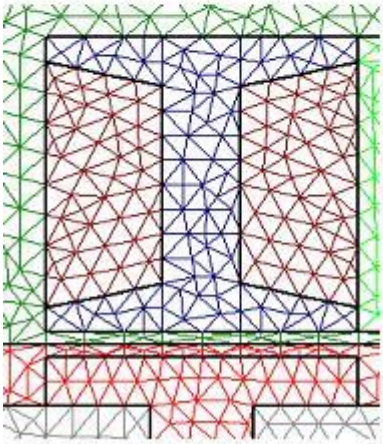

Fine Mesh

Figure 3.10: Core mesh density can be used in favor of a finer one in order to obtain accurate results

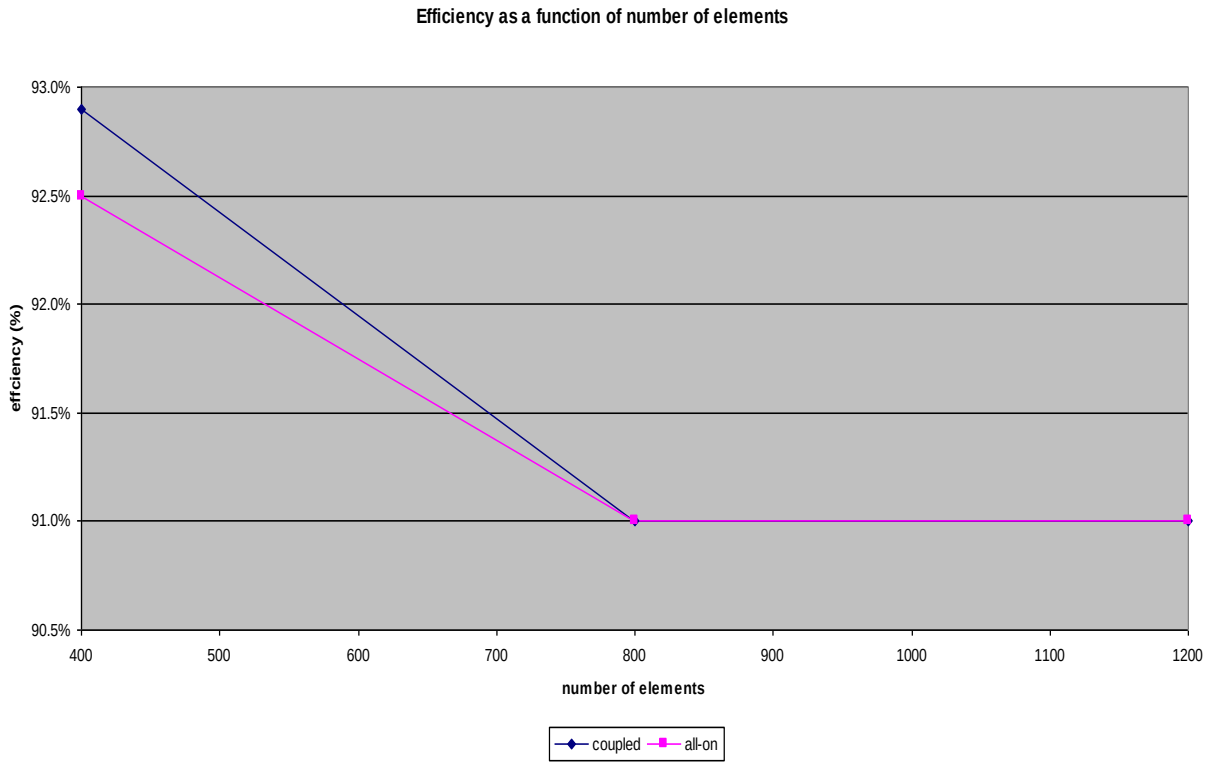

Figure 3.11: Comparison of efficiency for three different numbers of elements

3.3 Final results

After setting up the time step and the mesh size, the models representing the different topologies were run. Results are discussed in this section.

3.3.1 Thrust force

A plot of thrust force vs. velocity was generated for the different configurations studied at the velocities mentioned in section 2.3.5- Analysis Settings.

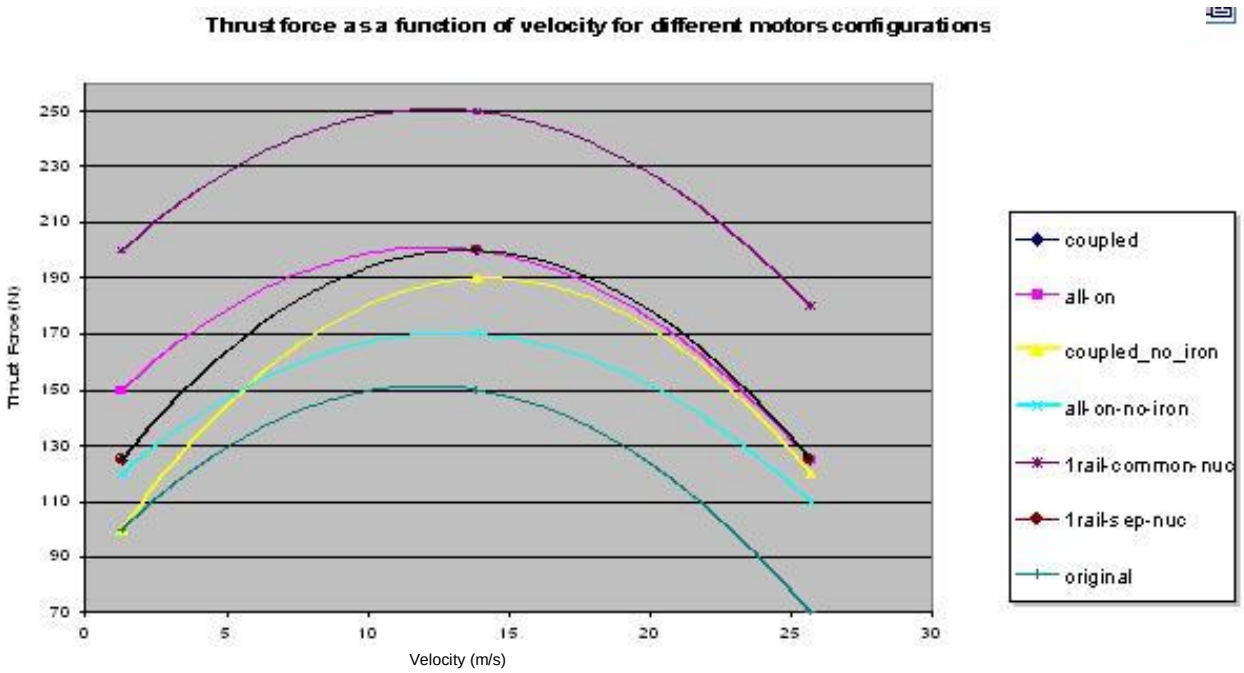

Figure 3.12: Thrust Force vs. Velocity for the investigated configurations

It can be seen that the configuration with the highest thrust force, 250 N, is the 1rail-common-nuc. This is the motor that contains the piece of iron at the top in such a way the entire nucleus are connected in between. A plot of the flux lines shows that flux lines in the order of 1.0e-3 Weber/m pass through the iron piece in such a way that coils receive more magnetic flux. As the magnetic flux is directly proportional to the Lorentz force, they can produce a higher thrust force.

3.3.2 Efficiency

A plot of efficiency vs. velocity was generated for the different configurations studied at the velocities mentioned in section 2.3.5- Analysis Settings.

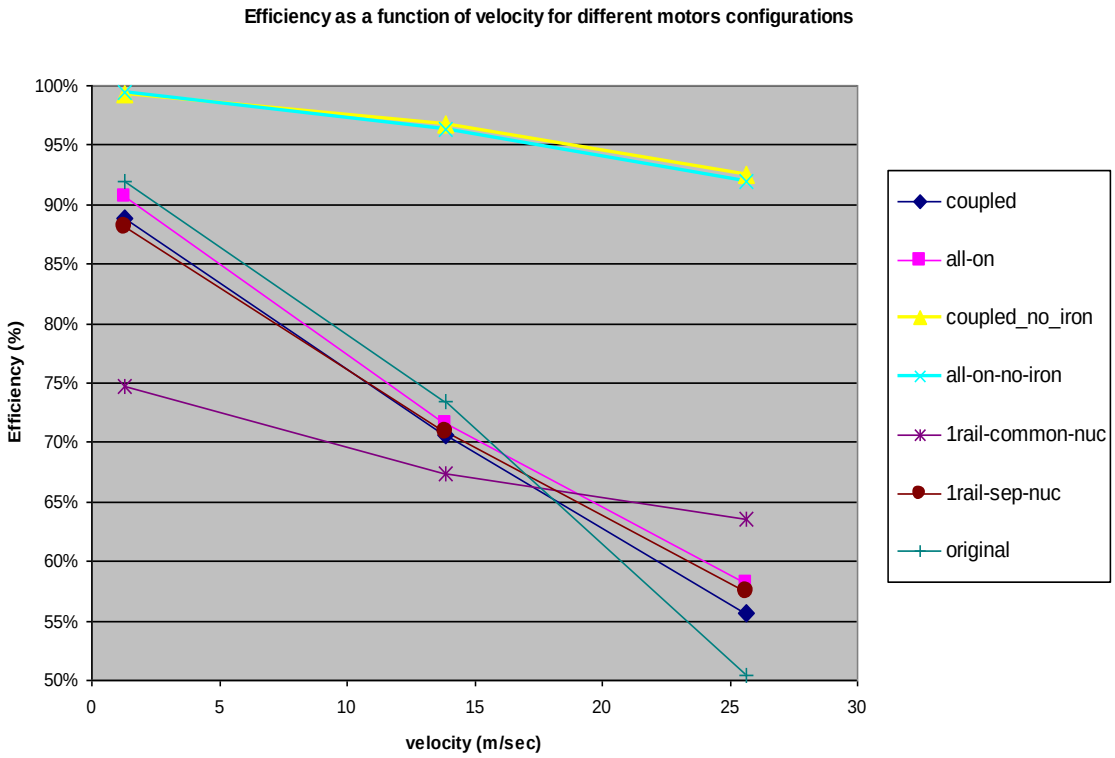

It can be seen that the configurations with the highest efficiencies, 99% are the ones that do not contain irons in the stator. If the flux lines contour plot is plotted for the motor with irons and without them, it can be noticed that there are additional flux lines in the irons that do not contribute to an increase in the magnetic flux in the moving members. Therefore, that additional flux means energy spent that is not used, i.e. more losses.

3.4 Effect of number of coils turns

One parameter that is very important in the design of the motors is the number of coil turns. The magnetic field increases proportional to this value, which means the force will increase but also the losses. Therefore, the number of coils that will satisfy the motor

operation is a compromise between force and efficiency. In this study, it was of interest to know the number of coils that will allow the motor to consume less power. The purpose of that is to obtain a baseline value that can be used in the manufacture of a prototype based on the Out-of-phase configuration. The number of coils turns selected was 80, 100, 110 and 120. Figure 3-13 shows that efficiency increase when the number of coils turns decrease. It is important that this analysis was done at constant volume, which means the geometry in the FE model was not modified. Also, it is deducted that different wire size should be used in the cable in order to accommodate the same volume.

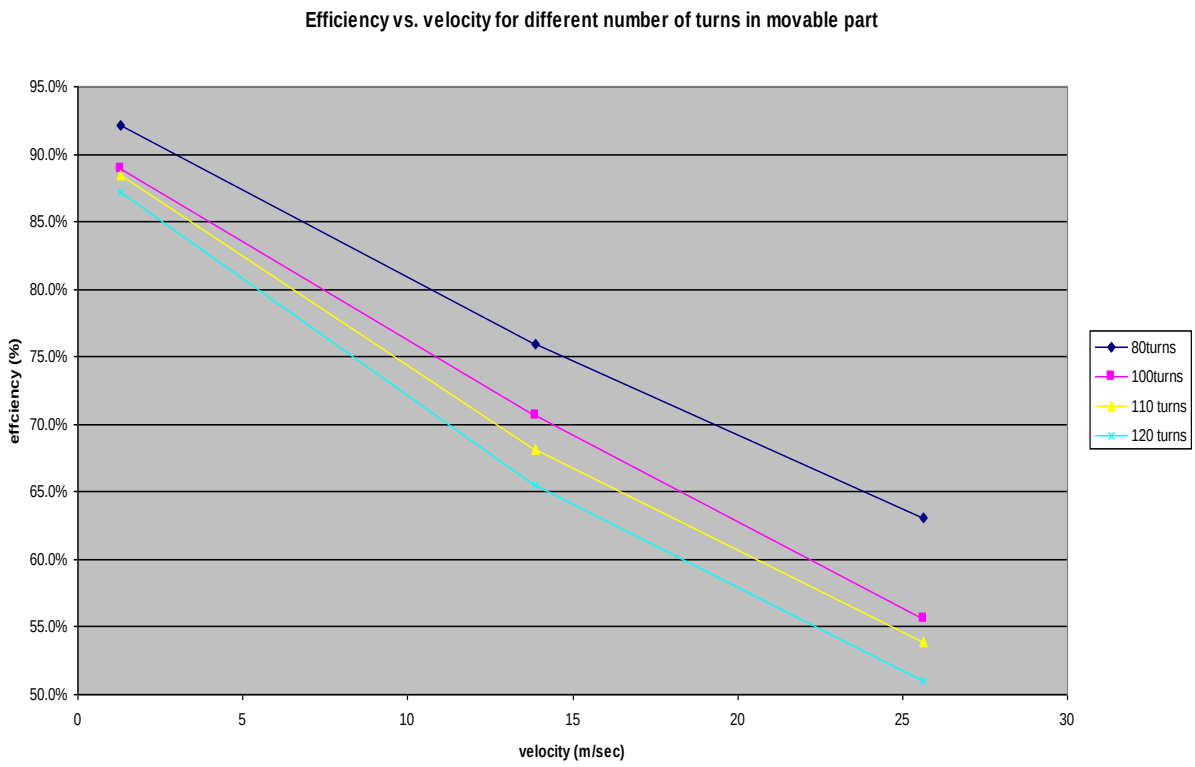

Figure 3.13: Effect of coils turns in efficiency for the Out-of-phase configuration

3.5 Effect of ripple

The way in which coils are positioned in the topologies with switching out-of-phase (coupled) and in-phase (all-on) suggested the generated thrust force will have different magnitude and frequency. This is due to the fact that in the first topology, three coils are generating force during the active (electrified) cycle and three of them by the passive (magnetic) one. Therefore, at any position, the thrust force will be a combination of the active and passive interaction. In the in-phase (all-on) configuration, the two switching cycles also contribute to the thrust at any given time. However, the expectation was that the coupled motor generates a force that runs smoother in time than the all-on motor and that both will contain approximately the same average force. Figure 3-14 shows the results. The thrust force is about the same frequency for both cases. In the in-phase (all-on) configuration the oscillations are of larger magnitude than in the out-of-phase (coupled). The line fit in this plot shows that both configurations perform similarly in ripple, with the out-of-phase slightly better.

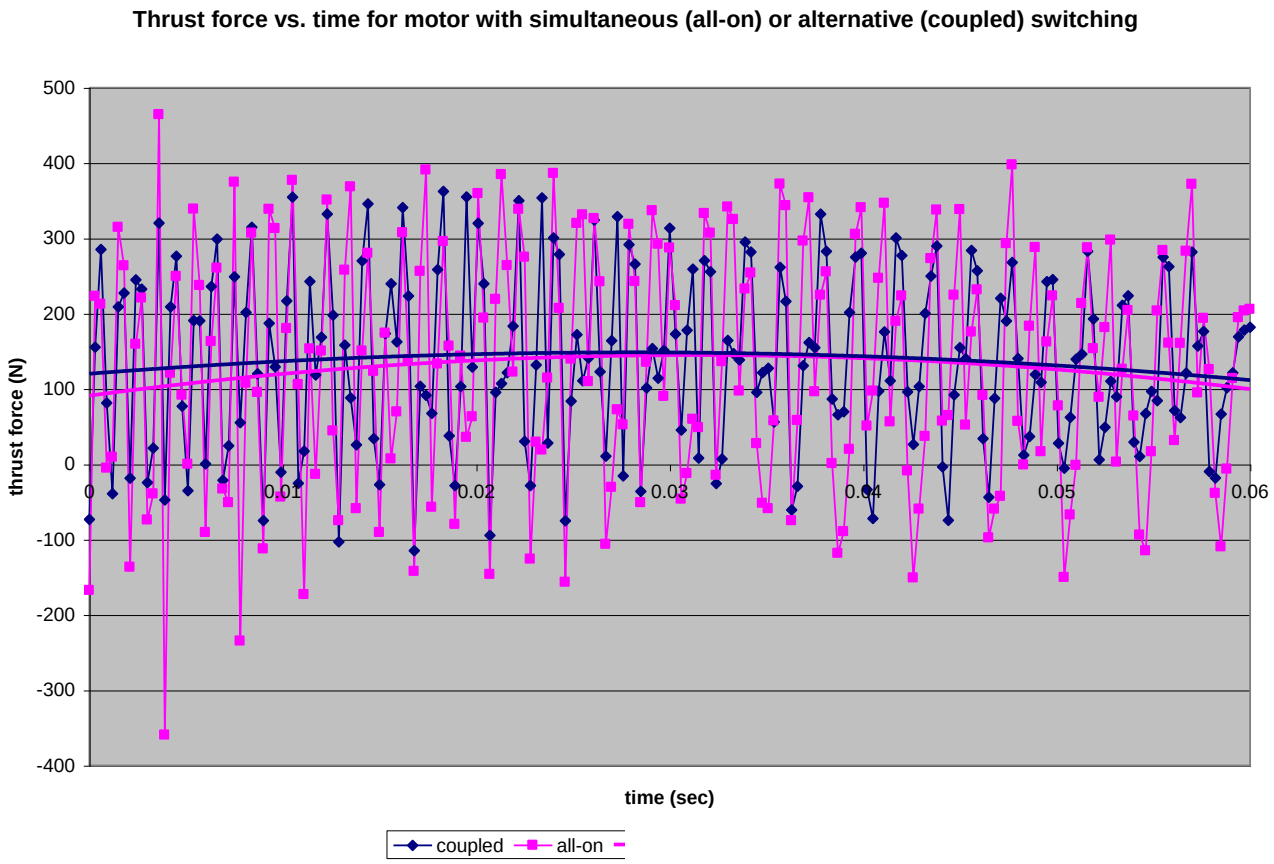

Figure 3.14: Thrust force vs. time used to investigate ripple between out-of-phase and in-phase configurations.

3.6 Performance comparison of Berdut linear motor and existing technologies

In the introduction was stated that the configurations assessed in this study will be compared with existing technologies. Two of these technologies will be reviewed in this section and compared with Berdut linear motor.

1. M3 MAGLEV system for Old Dominion University [25] – It is a development guideway located in Norfolk, VA. The propulsion is provided by a linear synchronous motor. In terms of weight, it has the capacity of 8,500 kg while Berdut carries only 1000 kg. That system can achieve a maximum velocity of 44.7 m/s, compared with Berdut in which the highest velocity at which it was simulated was 25.6 m/s. It can be expected that the Berdut motor will travel faster due have less weight but this is not the case. The reason for that might be the thrust load each of these motors can deliver. The maximum thrust for acceleration in the M3 is 16kN. It was not calculated acceleration in the Berdut motor but assuming constant velocity, that force reached 250 N. However, it can be shown the Berdut DC Linear Motor is more efficient than the M3. Maximum efficiency for Berdut is 99%, 19% more than the M3. Therefore, the Berdut motor has the potential to be competitive against existing linear motors used for propulsion in terms of the efficiency.
2. Linear Motors from MontiCont [26] – This is a company that designs linear motors for precision applications. The dimensions from their motors are similar to the ones of the Berdut configurations studied in this thesis. For example, the model LBF-241-01 has a width of 32 mm, a height of 57 mm and a length of 608 mm. Berdut has a width of 101 mm, a height of 25 mm and a length of 1400 mm. Comparing the output force for one of their models, the motor from MontiCont produces a maximum of 113.9 N. The lowest thrust force, achieved by the

coupled-no-iron and the original configurations was 100 N. Hence, the Berdut motor might operate in the same market these motors work.

4 CONCLUSIONS AND FUTURE WORK

4.1 Conclusions

In this thesis, the linear motor for train propulsion based on the Berdut technology was studied. Several topologies were investigated, along with the switching associated with them. A numerical model based on the Finite Element approach was developed using the Maxwell software. Based on the results of these models, it can be concluded that:

- Different linear motors configurations based in Berdut technology were evaluated in terms of thrust force and efficiency.
- The motor with one single rail and a common nucleus exhibits the highest thrust force = 250 N.
- The motors without iron in the stator provide the highest efficiencies, with a maximum of 99%. They maintain the same efficiency over a broader range, therefore offering more stable efficiency operation range.
- The time step selected, 1/200th of the simulation end time, allowed a combination of accuracy and speed in results is.
- The selected mesh density allowed less than 5% of error in the efficiency calculations.
- Efficiency has an inverse linear relationship with respect to the number of coils.

- There is no significant evidence on ripple effect between motors with simultaneous (all-on) and alternative (coupled) switching. However, it seems that there is a slight improvement in the alternate (coupled) motor.
- Berdut linear DC motor generates less thrust force than a selected commercial motor used in train propulsion but compares in others applications like precision machines. Efficiency is competitive against commercial motors used in train propulsion.

4.2 Future Work

Other considerations that should be taken into account for future work with this technology are:

1. Validate simulation results with experiments.
2. Explore performance of others topologies not presented in this work.
3. Perform shape optimization, once the best configuration of the layout topology is determined.
4. Analyze the performance of the active-passive configuration as a generator.
5. Explore other switching functions.

5 REFERENCES

[1] J. Reitz and F. Mildford, “Fundations of Electromagnetic Theory”, Addison-Wesley Pub. Comp., Massachusetts, 1967.

[2] E. Medici, “Finite Element Simulations and Optimization of Berdut Linear Motor for a Novel Elevator System”, Master Thesis, UPRM, Dec. 2005.

[3] J. Robles, “Dynamic Response and Damping Characteristics of a Berdut Skate for a Magnetically Levitated Train ”, Master Thesis, UPRM, Dec. 2003.

[4] http://www.oulu.fi/atkk/tkpalv/unix/ansys-6.1/content/thy_emg2.html

[5] Maxwell Online Help System. 1995-2004 Ansoft Corporation.

[6] M. A. Plonus, “Electromagnetismo Aplicado”, Ed. REVERTE S.A., Barcelona, Spain, 1992.

[7] P. Cambell, “Permanent Magnet Materials and their application”, Cambridge University Press, 1994

[8] http://en.wikipedia.org/wiki/Linear_motor

[9] http://www.wisegeek.com/what-are-the-different-types-of-electric-motors.htm

[10] http://www.oddparts.com/acsi/motortut.htm

[11] http://www.energy.wsu.edu/ftp-ep/pubs/engineering/motors/EfficiencyStandards.pdf
J. Douglass, “Induction Motor Efficiency Standards”, Washington State University Extension Energy Program

[12] “A Universal Motor Problem”, Ansoft RMxprt Application Note.

[13] R. Clarke. “Power losses in wound components”,
http://info.ee.surrey.ac.uk/Workshop/advice/coils/power_loss.html#hyst

[14] http://www.bharathtech.com/blog/uploaded_images/how-795586.gif

[15] http://www.rtri.or.jp/rd/maglev/html/english/maglev_frame_E.html

[16] E. Berdut, "Levitation and linear propulsion system using ceramic permanent magnets and interleaved malleable steel", U.S. Patent No 5.431.109, Jul. 1995.

[17] E. Berdut, "Levitation And Propulsion System Using Permanent Magnets And Interleaved Iron Or Steel", U.S. Patent No 5,452,633, Oct. 1994.
[18] E. Berdut, "Permanent magnet type automotive vehicle suspension", U.S. Patent No 5,584,367, Dec. 1996.

[19] E. Berdut, "Orbital and modular motors using permanent magnets and interleaved iron or steel magnetically permeable members", U.S. Patent No 5,615,618, Apr. 1997.

[20] www.physics.uiowa.edu/.../nov_06-04/motor.gif

[21] http://capital2.capital.edu/admin-staff/dalthoff/lim.html,
D. Althoff Jr., "Electric Voodoo: It's done with Magnets!", 2003

[22] http://www.mike-willis.com/Tutorial/PF2.htm

[23] http://my.execpc.com/~rhoadley/magmotor.htm

[24] http://en.wikipedia.org/wiki/Electromagnetic_induction

[25] An M3 Maglev System for Old Dominion University
No. 78 Richard Thornton, Tracy Clark, Brian Perreault, Jim Wieler, Steve Levine
MagneMotion Inc., 20 Sudbury Road, Acton, MA 01742, USA

[26] http://www.moticont.com/index.htm